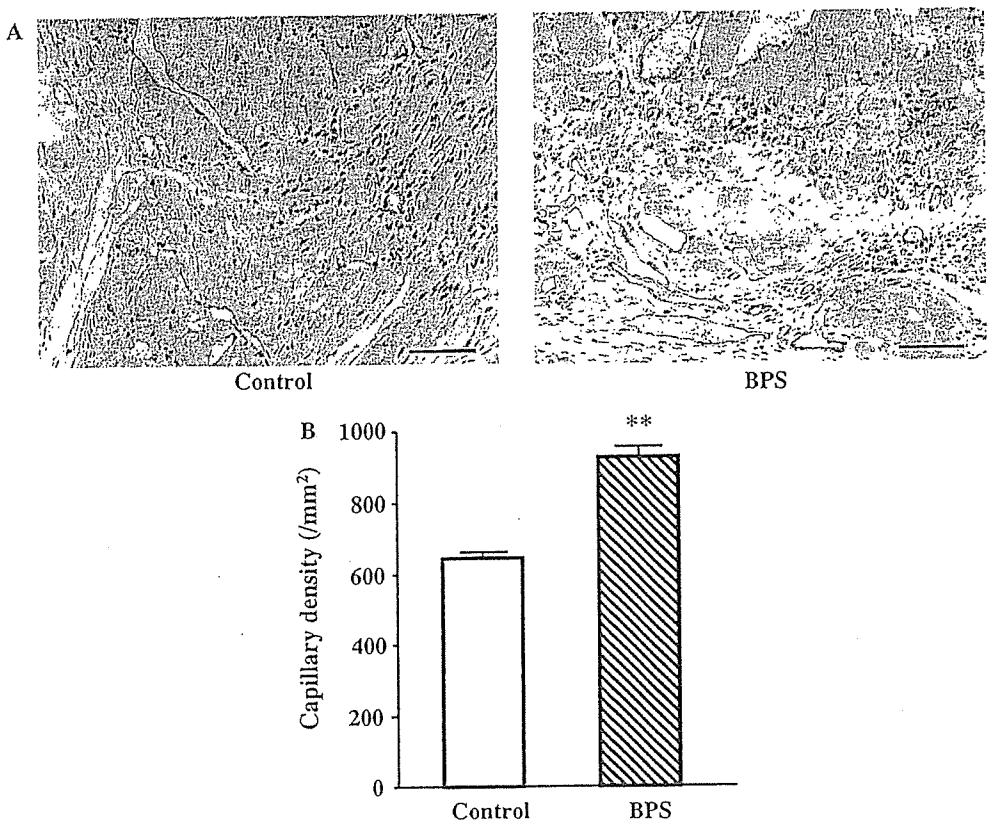

Fig. 5. (A) Representative samples stained with antibody to von Willebrand factor by bright-field DAB. (B) Quantitative analysis of capillary density in peri-infarct area. Administration of BPS increased capillary density by 37%. Scale bars = 50 μm. Data are expressed as means ± SEM. $^{**}p < 0.01$ vs. Control group.

Acknowledgment

This work was supported by research grants for Cardiovascular Disease (16C-6) from the Ministry of Health, Labor and Welfare, and for Japan Vascular Disease Research Foundation.

References

[1] A. Saraste, K. Pulkki, M. Kallajoki, K. Henriksen, M. Parvinen, L.M. Voipio-Pulkki, Apoptosis in human acute myocardial infarction, Circulation 95 (1997) 320–323.
[2] S. Shintani, T. Murohara, H. Ikeda, T. Ueno, T. Honma, A. Katoh, K. Sasaki, T. Shimada, Y. Oike, T. Imaizumi, Mobilization of endothelial progenitor cells in patients with acute myocardial infarction, Circulation 103 (2001) 2776–2779.
[3] D. Orlic, J. Kajstura, S. Chimenti, I. Jakoniuk, S.M. Anderson, B. Li, J. Pickel, R. Mckay, B. Nadal-Ginard, D.M. Bodine, A. Leri, P. Anversa, Bone marrow cells regenerate infarcted myocardium, Nature 410 (2001) 701–705.
[4] H. Oh, S.B. Bradfute, T.D. Gallardo, T. Nakamura, V. Gaussin, Y. Mishina, J. Pocius, L.H. Michael, R.R. Behringer, D.J. Garry, M.L. Entman, M.D. Schneider, Cardiac progenitor cells from adult myocardium: homing, differentiation, and fusion after infarction, Proc. Natl. Acad. Sci. USA 100 (2003) 12313–12318.
[5] D. Orlic, J. Kajstura, S. Chimenti, F. Limana, I. Jakoniuk, F. Quaini, B. Nadal-Ginard, D.M. Bodine, A. Leri, P. Anversa, Mobilized bone marrow cells repair the infarcted heart, improving function and survival, Proc. Natl. Acad. Sci. USA 98 (2001) 10344–10349.
[6] T. Asahara, T. Takahashi, H. Masuda, C. Kalka, D. Chen, H. Iwaguro, Y. Inai, M. Silver, J.M. Isner, VEGF contributes to postnatal neovascularization by mobilizing bone marrow-derived endothelial progenitor cells, EMBO J. 18 (1999) 3964–3972.
[7] T. Murata, T. Murai, T. Kanai, Y. Ogaki, K. Sanai, H. Kanda, S. Sato, N. Kajikawa, T. Umetsu, H. Matsuura, General pharmacology of beraprost sodium, Arzneimittelforschung 39 (1989) 867–876.
[8] T. Akiba, M. Miyazaki, N. Toda, Vasodilator actions of TRK-100, a new prostaglandin I2 analogue, Br. J. Pharmacol. 89 (1986) 703–711.
[9] S. Nishio, H. Matsuura, N. Kanai, Y. Fukatsu, T. Hirano, N. Nishikawa, K. Kameoka, T. Umetsu, The in vitro and ex vivo antiplatelet effect of TRK-100, a stable prostacyclin analog, in several species, Jpn J. Pharmacol. 47 (1988) 1–10.
[10] J.L. Demolis, A. Robert, M. Mouren, C. Funck-Brentano, P. Jaillon, Pharmacokinetics and platelet antiaggregating effects of beraprost, an oral stable prostacyclin analogue, in healthy volunteers, J. Cardiovasc. Pharmacol. 22 (1993) 711–716.
[11] P. Nony, P. Ffrench, P. Girard, S. Delair, S. Azoulay, J.P. Girre, M. Dechavanne, J.P. Boissel, Platelet-aggregation inhibition and hemodynamic effects of beraprost sodium, a new oral prostacyclin derivative: a study in healthy male subjects, Can. J. Physiol. Pharmacol. 74 (1996) 887–893.
[12] M. Murakami, M. Watanabe, H. Furukawa, H. Nakahara, The prostacyclin analogue beraprost sodium prevents occlusion of bypass grafts in patients with lower extremity arterial occlusive disease: a 20-year retrospective study, Ann. Vasc. Surg. 19 (2005) 838–842.
[13] L.T. Cooper, Beraprost for the treatment of intermittent claudication, J. Am. Coll. Cardiol. 41 (2003) 1679–1686.
[14] Y. Okano, T. Yoshioka, A. Shimouchi, T. Satoh, T. Kunieda, Orally active prostacyclin analogue in primary pulmonary hypertension, Lancet 349 (1997) 1365.

[15] N. Nagaya, M. Uematsu, Y. Okano, T. Satoh, S. Kyotani, F. Sakamaki, N. Nakanishi, K. Miyatake, T. Kunieda, Effect of orally active prostacyclin analogue on survival of outpatients with primary pulmonary hypertension, J. Am. Coll. Cardiol. 34 (1999) 1188–1192.
[16] A.M. Lefer, M.L. Ogletree, J.B. Smith, M.J. Silver, K.C. Nicolaou, W.E. Barnette, G.P. Gasic, Prostacyclin: a potentially valuable agent for preserving myocardial tissue in acute myocardial ischemia, Science 200 (1978) 52–54.
[17] B.I. Jugdutt, G.M. Hutchins, B.H. Bulkley, L.C. Becker, Dissimilar effects of prostacyclin, prostaglandin E1, and prostaglandin E2 on myocardial infarct size after coronary occlusion in conscious dogs, Circ. Res. 49 (1981) 685–700.
[18] J.A. Melin, L.C. Becker, Salvage of ischemic myocardium by prostacyclin during experimental myocardial infarction, J. Am. Coll. Cardiol. 2 (1983) 279–286.
[19] K. Niwano, M. Arai, K. Tomaru, T. Uchiyama, Y. Ohyama, M. Kurabayashi, Transcriptional stimulation of the eNOS gene by the stable prostacyclin analogue beraprost is mediated through cAMP-responsive element in vascular endothelial cells: close link between PGI2 signal and NO pathways, Circ. Res. 93 (2003) 523–530.
[20] A. Aicher, C. Heeschen, C. Mildner-Rihm, C. Urbich, C. Ihling, K. Technau-Ihling, A.M. Zeiher, S. Dimmeler, Essential role of endothelial nitric oxide synthase for mobilization of stem and progenitor cells, Nat. Med. 9 (2003) 1370–1376.
[21] T. Nishikimi, K. Uchino, E.D. Frohlich, Effects of α1-adrenergic blockade on intrarenal hemodynamics in heart failure rats, Am. J. Physiol. Regul. Integr. Comp. Physiol. 262 (1998) R198–R203.
[22] P.S. Douglas, N. Reichek, T. Plappert, A. Muhammad, M.G. St John Sutton, Comparison of echocardiographic methods for assessment of left ventricular shortening and wall stress, J. Am. Coll. Cardiol. 9 (1987) 945–951.
[23] Y.W. Chien, R.W. Barbee, A.A. Macphee, E.D. Frohlich, N.C. Trippondo, Increased ANF secretion after volume expansion is preserved in rats with heart failure, Am. J. Physiol. 254 (1988) R185–R191.
[24] T. Ito, A. Suzuki, E. Imai, M. Okabe, M. Hori, Bone marrow is a reservoir of repopulating mesangial cells during glomerular remodeling, J. Am. Soc. Nephrol. 12 (2001) 2625–2635.
[25] P.J. Simpson, R.F. Todd 3rd, J.C. Fantone, J.K. Mickelson, J.D. Griffin, B.R. Lucchesi, Reduction of experimental canine myocardial reperfusion injury by a monoclonal antibody (anti-Mo1, anti-CD11b) that inhibits leukocyte adhesion, J. Clin. Invest. 81 (1988) 624–629.
[26] W.W. Nichols, J. Mehta, T.J. Wargovich, D. Franzini, D. Lawson, Reduced myocardial neutrophil accumulation and infarct size following thromboxane synthetase inhibitor or receptor antagonist, Angiology 40 (1989) 209–221.
[27] M. Kainoh, R. Imai, T. Nakadake, M. Hattori, S. Nishio, Prostacyclin and beraprost sodium as suppressors of activated rat polymorphonuclear leukocytes, Biochem. Pharmacol. 39 (1990) 477–483.
[28] Y. Ueno, Y. Miyauchi, S. Nishio, Beraprost sodium protects occlusion/reperfusion injury in the dog by inhibition of neutrophil migration, Gen. Pharmacol. 25 (1994) 427–432.
[29] A. Kawamoto, T. Tkebuchava, J. Yamaguchi, H. Nishimura, Y.S. Yoon, C. Milliken, S. Uchida, O. Masuo, H. Iwaguro, H. Ma, A. Hanley, M. Silver, M. learney, D.W. Losordo, J.M. Isner, T. Asahara, Intramyocardial transplantation of autologous endothelial progenitor cells for therapeutic neovascularization of myocardial ischemia, Circulation 107 (2003) 461–468.
[30] A. Kawamoto, T. Asahara, D.W. Losordo, Transplantation of endothelial progenitor cells for therapeutic neovascularization, Cardiovasc. Radiat. Med. 3 (2002) 221–225.
[31] A. Weber, I. Pedrosa, A. Kawamoto, N. Himes, J. Munasinghe, T. Asahara, N.M. Rofsky, D.W. Losordo, Magnetic resonance mapping of transplanted endothelial progenitor cells for therapeutic neovascularization in ischemic heart disease, Eur. J. Cardiothorac. Surg. 26 (2004) 137–143.
[32] J. Kajstura, M. Rota, B. Whang, S. Cascapera, T. Hosoda, C. Bearzi, D. Nurzynska, H. Kasahara, E. Zias, M. Bonafe, B. Nadal-Ginard, D. Torella, A. Nascimbene, F. Quaini, K. Urbanek, A. Leri, P. Anversa, Bone marrow cells differentiate in cardiac cell lineages after infarction independently of cell fusion, Circ. Res. 96 (2005) 127–137.
[33] R. Lanza, M.A. Moore, T. Wakayama, A.C. Perry, J.H. Shieh, J. Hendrikx, A. Leri, S. Chimenti, A. Monsen, D. Nurzynska, M.D. West, J. Kajstura, P. Anversa, Regeneration of the infarcted heart with stem cells derived by nuclear transplantation, Circ. Res. 94 (2004) 820–827.
[34] Y. Uchida, T. Hanai, K. Hasegawa, K. Kawamura, T. Oshima, Recanalization of obstructed coronary artery by intracoronary administration of prostacyclin in patients with acute myocardial infarction, Adv. Prostaglandin Thromboxane Leukot. Res. 11 (1983) 377–383.
[35] C.Y. Xiao, A. Hara, Yuhki K, T. Fujino, H. Ma, Y. Okada, O. Takahata, T. Yamada, T. Murata, S. Narumiya, F. Ushikubi, Roles of prostaglandin I(2) and thromboxane A(2) in cardiac ischemia–reperfusion injury: a study using mice lacking their respective receptors, Circulation 104 (2001) 2210–2215.
[36] A. Szczeklik, J. Szczeklik, R. Nizankowski, P. Gluszko, Prostacyclin for unstable angina, N. Engl. J. Med. 303 (1980) 881.
[37] M.L. Knudtson, V.F. Flintoft, D.L. Roth, J.L. Hansen, H.J. Duff, Effect of short-term prostacyclin administration on restenosis after percutaneous transluminal coronary angioplasty, J. Am. Coll. Cardiol. 15 (1990) 691–697.
[38] F. Kuethe, H.R. Figulla, M. Herzau, M. Voth, M. Fritzenwanger, T. Opfermann, K. Pachmann, A. Krack, H.G. Sayer, D. Gottschild, G.S. Werner, Treatment with granulocyte colony-stimulating factor for mobilization of bone marrow cells in patients with acute myocardial infarction, Am. Heart J. 150 (2005) 115.
[39] H.J. Kang, H.S. Kim, S.Y. Zhang, K.W. Park, H.J. Cho, B.K. Koo, Y.J. Kim, D. Soo Lee, D.W. Sohn, K.S. Han, B.H. Oh, M.M. Lee, Y.B. Park, Effects of intracoronary infusion of peripheral blood stem-cells mobilised with granulocyte-colony stimulating factor on left ventricular systolic function and restenosis after coronary stenting in myocardial infarction: the MAGIC cell randomised clinical trial, Lancet 363 (2004) 751–756.
[40] R.M. Califf, K.F. Adams, W.J. McKenna, M. Gheorghiade, B.F. Uretsky, S.E. McNulty, H. Darius, K. Schulman, F. Zannad, E. Handberg-Thurmond, F.E. Harrell Jr., W. Wheeler, J. Soler-Soler, K. Swedberg, A randomized controlled trial of epoprostenol therapy for severe congestive heart failure: The Flolan International Randomized Survival Trial (FIRST), Am. Heart J. 134 (1997) 44–54.
[41] M. Lievre, S. Morand, B. Besse, J.N. Fiessinger, J.P. Boissel, Oral beraprost sodium, a prostaglandin I(2) analogue, for intermittent claudication: a double-blind, randomized, multicenter controlled trial. Beraprost et Claudication Intermittente (BERCI) Research Group, Circulation 102 (2000) 426–431.
[42] E.R. Mohler 3rd, W.R. Hiatt, J.W. Olin, M. Wade, R. Jeffs, A.T. Hirsch, Treatment of intermittent claudication with beraprost sodium, an orally active prostaglandin I2 analogue: a double-blinded, randomized, controlled trial, J. Am. Coll. Cardiol. 41 (2003) 1679–1686.

Unblinded Pilot Study of Autologous Transplantation of Bone Marrow Mononuclear Cells in Patients With Thromboangiitis Obliterans

Koji Miyamoto, MD; Kazuhiro Nishigami, MD; Noritoshi Nagaya, MD; Koichi Akutsu, MD; Masaaki Chiku, MD; Masataka Kamei, MD; Toshihiro Soma, MD; Shigeki Miyata, MD; Masahiro Higashi, MD; Ryoichi Tanaka, MD; Takeshi Nakatani, MD; Hiroshi Nonogi, MD; Satoshi Takeshita, MD

Background—The short-term clinical benefits of bone marrow mononuclear cell transplantation have been shown in patients with critical limb ischemia. The purpose of this study was to assess the long-term safety and efficacy of bone marrow mononuclear cell transplantation in patients with thromboangiitis obliterans.

Methods and Results—Eleven limbs (3 with rest pain and 8 with an ischemic ulcer) of 8 patients were treated by bone marrow mononuclear cell transplantation. The patients were followed up for clinical events for a mean of 684±549 days (range 103 to 1466 days). At 4 weeks, improvement in pain was observed in all 11 limbs, with complete relief in 4 (36%). Pain scale (visual analog scale) score decreased from 5.1±0.7 to 1.5±1.3. An improvement in skin ulcers was observed in all 8 limbs with an ischemic ulcer, with complete healing in 7 (88%). During the follow-up, however, clinical events occurred in 4 of the 8 patients. The first patient suffered sudden death at 20 months after transplantation at 30 years of age. The second patient with an incomplete healing of a skin ulcer showed worsening of the lesion at 4 months. The third patient showed worsening of rest pain at 8 months. The last patient developed an arteriovenous shunt in the foot at 7 months, which spontaneously regressed by 1 year.

Conclusions—In the present unblinded and uncontrolled pilot study, long-term adverse events, including death and unfavorable angiogenesis, were observed in half of the patients receiving bone marrow mononuclear cell transplantation. Given the current incomplete knowledge of the safety and efficacy of this strategy, careful long-term monitoring is required for future patients receiving this treatment. (*Circulation*. 2006;114:2679-2684.)

Key Words: angiogenesis ■ collateral circulation ■ endothelium ■ peripheral vascular diseases

The clinical consequences of severe peripheral arterial disease or critical limb ischemia include rest pain and the loss of tissue integrity in the distal limb.[1–3] Therapeutic options for such patients are limited. These conditions are often refractory to conservative measures and are typically unresponsive to drug therapy. When vascular obstruction involves a long segment or is widespread, percutaneous revascularization may not be feasible. Surgical therapy, consisting of arterial bypass or amputation, is complicated by variable morbidity and mortality, and its effectiveness depends on the short- and long-term patencies of the conduit employed. Therapeutic angiogenesis thus constitutes a potential alternative treatment strategy for such patients.[4,5]

Previous investigators have suggested that endothelial progenitor cells, originating from bone marrow, circulate in adult peripheral blood and participate in postnatal neovascularization.[6–8] Subsequent experiments have shown that bone marrow or bone marrow–derived cells have the potential to stimulate angiogenesis and thereby modulate the hemodynamic deficit in ischemic limbs in vivo.[9,10] The Therapeutic Angiogenesis by Cell Transplantation (TACT) study first demonstrated that the magnitude of angiogenesis stimulated by these cells is sufficient to constitute a therapeutic benefit in patients with critical limb ischemia.[11] In that study, the investigators injected bone marrow mononuclear cells (BM-MNCs) into the ischemic limb of patients and documented a significant improvement in the hemodynamic deficit as well as the relief of ischemic symptoms. Although the TACT

Editorial p 2581
Clinical Perspective p 2684

Received June 9, 2006; revision received September 19, 2006; accepted September 21, 2006.

From the Departments of Medicine (K.M., K.N., K.A., M.C., H.N., S.T.), Regenerative Medicine and Tissue Engineering (N.N.), Anesthesiology (M.K.), Transfusion Medicine (S.M.), Radiology (M.H., R.T.), and Organ Transplantation (T.N.), National Cardiovascular Center, Osaka; and the Department of Clinical Laboratory (T.S.), Osaka Minami Medical Center, Osaka, Japan.

Correspondence to Dr Satoshi Takeshita, MD, FACC, Department of Medicine (Cardiology), National Cardiovascular Center, 5-7-1 Fujishiro-dai, Suita, Osaka 565-8565, Japan. E-mail stake@muse.ocn.ne.jp

Circulation is available at http://www.circulationaha.org

DOI: 10.1161/CIRCULATIONAHA.106.644203

study established the concept of using BM-MNCs for therapeutic angiogenesis, limited information is available about the long-term safety and efficacy of this strategy.

The purpose of the present study was to determine the long-term safety and clinical impact of BM-MNC transplantation for "no-option" patients with thromboangiitis obliterans.

Methods

Patients

Eight patients with thromboangiitis obliterans were treated with an autologous transplantation of BM-MNCs between March 2002 and September 2004. The diagnosis of thromboangiitis obliterans was based on the criteria proposed by Olin[12]: (1) onset before age 45; (2) current (recent) history of tobacco use; (3) the presence of distal-extremity ischemia (infrapopliteal or infrabrachial) indicated by claudication, rest pain, ischemic ulcers, or gangrene; (4) exclusion of autoimmune or connective tissue diseases, hypercoagulable states, and diabetes mellitus; (5) exclusion of a proximal source of emboli by echocardiography and arteriography; and (6) consistent arteriographic findings in the clinically involved and noninvolved limbs.

Patients qualified for cell transplantation if they had chronic limb ischemia, with rest pain or a nonhealing ischemic ulcer, present for a minimum of 4 weeks without evidence of improvement in response to conventional drug therapy; showed angiographic evidence of vasculopenia in the affected limb; and were not candidates for percutaneous or surgical revascularization. The exclusion criteria included severe concurrent illness, the presence of proliferative diabetic retinopathy, and a history or clinical evidence of a malignant disorder.

All the patients involved in the present study received continuous medical therapy for >2 months before BM-MNC transplantation to confirm that conventional measures would be insufficient to achieve improvement in rest pain or skin ulcer/gangrene. During this period, no surgical therapies such as bypass grafting, extensive debridement, skin grafting, or limb amputation were performed. In addition, the patients were admitted to the hospital for a minimum of 1 month before BM-MNC transplantation to exclude the likelihood of spontaneous improvement in ischemic symptoms resulting from an enrollment bias. It should be also pointed out that the patients remained in the hospital and received the same therapy for at least 1 month after BM-MNC transplantation to avoid changes in their treatment.

BM-MNC Transplantation

While the patients were under general anesthesia, marrow cells were aspirated from the ileum. BM-MNCs were sorted on an AS-104 blood-cell separator (Fresenius HemoCare, Redmond, Wash) and concentrated to a final volume of ≈50 mL. After bone marrow cells were sorted on the AS-104 blood-cell separator, a small fraction of the cells was used for BM-MNC counting; the concentration of BM-MNCs in the final product was determined by using a microscope counting chamber after May-Giemsa staining. By using another fraction of cells, the number of $CD34^+$ cells in the BM-MNCs was also determined by fluorescence-activated cell sorting (FACS SCAN flow cytometer; Becton Dickinson, San Jose, Calif). The cells were incubated with the FITC-conjugated mouse monoclonal antibody against human CD34 (clone 581; Becton Dickinson) according to manufacturer's instructions.

For each patient, ≈100 aliquots of BM-MNCs (0.5 mL per aliquot) were administered via a syringe with a 27-gauge needle. Injection was performed into 9 lower limbs in 7 of the patients and the bilateral hands in 1. Injection sites were arbitrarily selected according to angiographic findings (ie, the degree of vasculopenia) and included calf muscles such as the soleus and gastrocunemius muscles as well as the sole muscles of the foot. For the patient with hand ischemia, injection was performed in palm muscles.

Assessment of Short-Term Outcome

Ischemic pain was assessed with a visual analog pain scale (VAS) with 10 levels. Ischemic ulcers were documented by color photography. Resting ankle-brachial pressure index (ABI) was calculated as the quotient of absolute ankle pressure and brachial pressure (the patient who received BM-MNC transplantation in his hands was excluded from ABI analysis). Angiographic assessment was performed with magnetic resonance angiography, computed tomographic angiography, or digital subtraction angiography. Adverse events were defined as death, limb amputation, pathological angiogenesis, recurrence/worsening of ischemic symptoms (ie, rest pain, skin ulcer, gangrene), myocardial infarction, stroke, and malignant disease.

Assessment of Long-Term Outcome

The mean length of follow-up was 684±549 days (range 103 to 1466). Patients were followed up by history analysis, physical examination, routine blood testing, ABI, and angiography at prescribed intervals during the first year, after which they were contacted at an outpatient clinic or by telephone to track events.

Data Analysis

All data are presented as mean±SD (range) or frequencies (percentage).

The authors had full access to and take full responsibility for the integrity of the data. All authors have read and agree to the manuscript as written.

Results

Diagnosis

The diagnosis of thromboangiitis obliterans was made according to the criteria described above. Among the 8 patients, only patient 6 did not completely fulfill the criteria; ie, this patient had no history of tobacco use (Table 1). Laboratory screening excluded the possibility of other underlying diseases, however, including autoimmune and connective tissue diseases. It should be also pointed out that patient 6 had diabetes mellitus at the time of cell transplantation but not at the onset of thromboangiitis obliterans. With the typical characteristic angiographic findings of thromboangiitis obliterans, such as multiple segmental arterial involvement (skip lesions) and "cork-screw" collateral vessels, we diagnosed patient 6 as having thromboangiitis obliterans, even though the patient did not have a history of tobacco use.

Patient Characteristics

The demographic and clinical data of the 8 patients are shown in Table 1. The mean age of the patients enrolled was 46±14 years (range 28 to 63). Seven patients (88%) were male. One patient had undergone prior femoral-tibial artery bypass grafting, and 1 had undergone sympathetic ganglion block. These treatments were performed >1 year before BM-MNC transplantation. Seven patients (88%) had a history of smoking, all of whom stopped smoking at least 1 month before transplantation.

Short-Term Outcome

The total volume of cells aspirated from the ileum was 728±72 mL (range 600 to 800) per patient, and the total volume of injected BM-MNCs was 45±7 mL (range 30 to 50) per patient. Total number of injected BM-MNCs was $3.5\pm0.8\times10^9$ (range 2.0 to 4.7×10^9), and that of $CD34^+$ cells was $6.8\pm2.6\times10^7$ (range 2.4 to 9.7×10^7).

TABLE 1. Patient Characteristics

Patient	Age	Sex	Fontaine Stage	Previous Treatment	DM	HT	HLP	Smoking	BM-MNC ($\times 10^9$)	$CD34^+$ in BM-MNC ($\times 10^7$)	ABI, Baseline	ABI, 1 Month	VAS, Baseline	VAS, 1 Month
1	63	M	III(lt)	Bypass graft	−	−	+	+	3.0	6.6	0.34	0.55	5	0
2	31	M	IV(rt)	Medical	−	−	−	+	4.7	9.7	0.49	0.39	5	1
3	52	M	IV(lt)	Medical	−	−	−	+	4.1	9.0	0.65	0.67	7	2
4	28	M	IV(lt)	Sympathetic ganglion block	−	−	−	+	2.0	6.8	0.50	0.26	5	0
5	32	M	IV(rt)	Medical	−	−	−	+	3.8	2.4	−	−	5	2
			IV(lt)								−	−	5	2
6	55	F	IV(lt)	Medical	+	+	−	−	3.4	4.0	0.53	0.51	4	3
7	63	M	III(rt)	Medical	−	+	−	+	3.0	9.1	1.10	0.91	5	3
			IV(lt)								0.76	0.94	5	3
8	43	M	IV(rt)	Medical	−	+	−	+	3.6	6.8	1.00	1.04	5	0
			III(lt)								1.00	1.07	5	0

DM indicates diabetes mellitus; HT, hypertension; and HLP, hyperlipidemia.

Angiographic assessment at 4 weeks after transplantation revealed an apparent increase in limb vascularity in 3 of the 8 (38%) patients (4 of the 11 limbs) (Figure 1). Hemodynamic assessment also failed to document evidence of improved collateral development. Specifically, an increase in ABI (>0.1) was observed in 2 of 7 (29%) patients (2 of 8 limbs), whereas a decrease in ABI (>0.1) was observed in 2 of 7 (29%) patients (2 of 8 limbs). As a result, mean ABI measured at 4 weeks (0.71±0.30) did not differ from that at the baseline (0.70±0.27). Because 2 patients had sites of arterial occlusion distal to the ankle, they showed normal ABIs before treatment. Even after the exclusion of these 2 patients, ABI showed no changes between before (0.55±0.15) and after transplantation (0.55±0.24).

In contrast to the angiographic and hemodynamic results, improvement in limb status was observed in all 8 patients (100%). Improvement in VAS was observed in all 11 limbs, with a decrease from a mean of 5.1±0.7 to 1.5±1.3. Furthermore, complete pain relief was achieved in 4 of the 11 limbs (36%). Improvement in skin ulcers was also observed in all 8 limbs (100%), with complete healing in 7 (88%). Although surgical amputations of the distal limb were performed in 2 patients at 1 month, these operations were intentionally scheduled to be performed after transplantation with the expectation of sufficiently improving the limb perfusion to distally advance the site of amputation (Table 2; Figure 2A and 2B).

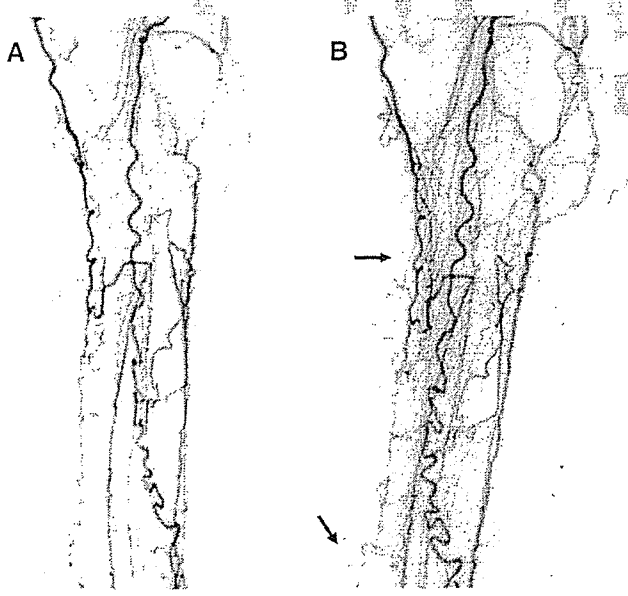

Figure 1. Digital subtraction angiography at (A) baseline and (B) 1 month after cell transplantation. Arrows indicate newly visible collateral vessels at the calf level.

Long-Term Outcome

The mean follow-up period was 684±549 days (range 103 to 1466). At the final follow-up, VAS score remained unchanged from that observed at 1 month after transplantation in 5 of the 8 patients (63%). The mean VAS score at follow-up also remained low (2.3±1.9) compared with that observed at baseline (5.1±0.7).

In contrast to the pain scale results, adverse events were observed in as many as 4 patients (50%) (Table 2). At age 30

TABLE 2. Adverse Outcomes After Autologous Transplantation of BM-MNCs in Patients With Thromboangiitis Obliterans

Adverse Outcomes	30 Days	Final Follow-Up
Death	0	1 (13)
Major amputation	0	0
Minor amputation	2 (25)*	0
Unexpected angiogenesis	0	1 (13)
Recurrence/worsening of skin ulcer/gangrene	0	2 (25)†
Recurrence/worsening of pain	0	1 (13)
Cardiovascular event	0	0
Cerebrovascular event	0	0
Malignancy	0	0

Values are expressed as n (%).

*Amputation was intentionally scheduled to be performed at 1 month after transplantation.

†One patient was the same one who developed unexpected angiogenesis.

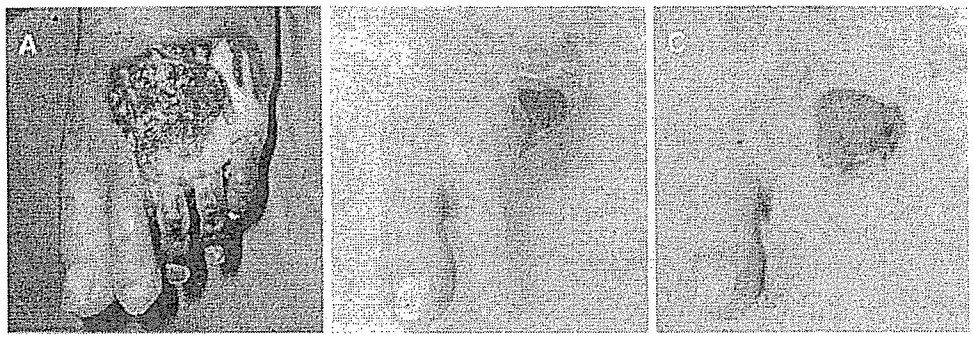

Figure 2. Skin ulcer at (A) 1 month, (B) 2 months, and (C) 4 months after cell transplantation. The patient had far-advanced gangrene, and total limb integrity could not be fully preserved. The patient received a prescheduled amputation of the distal limb at 1 month, and the skin ulcer continued to improve thereafter. At 4 months, however, the skin lesion began to enlarge.

years, patient 4 suddenly died of an unknown cause at 20 months after transplantation. This patient had previously been a smoker, but had stopped smoking before cell transplantation. He had no history of diabetes, hypertension, or hyperlipidemia. Furthermore, ^{201}thallium myocardial scan performed before BM-MNC transplantation showed no signs of myocardial ischemia. After cell transplantation, his limb pain disappeared within 1 week and his skin ulcer resolved by 1 month. Thereafter, he was completely free of limb symptoms. Twenty months after cell transplantation, however, he was found dead at his home. He had never experienced chest pain up to the time of his death. Because no autopsy was performed, the cause of his death remains unknown.

Patient 6 showed worsening of an ischemic ulcer at 4 months. The patient had far-advanced gangrene, and total limb integrity could not be fully preserved. The patient underwent a prescheduled amputation of the distal limb at 1 month (see Short-Term Outcome) (Figure 2A), and the skin ulcer continued to improve thereafter (Figure 2B). At 4 months, however, the skin lesion began to increase in size (Figure 2C). The patient subsequently received a second round of cell therapy.

In patient 7, despite complete healing of the skin ulcer, rest pain did not completely resolve after transplantation, with a VAS score of 3 at 1 month. At 8 months, the patient experienced worsening of rest pain (VAS score=4). After a combination of exercise training and maximal drug therapy, the pain improved and became well tolerated.

Patient 8 experienced swelling and recurrence of the skin ulcer in his foot at 7 months. Computed tomographic angiography documented an early venous return of contrast material in his right limb (Figure 3B) that was not observed at the baseline (Figure 3A). Ultrasound examination disclosed an arterialized waveform in the dorsal vein at the base of his third toe, suggesting the presence of an arteriovenous shunt. By 1 year, the swelling and skin ulcer had spontaneously regressed. The systolic pulsatile component in the venous waveform was found to be diminished on ultrasound examination, and early venous filling had disappeared on computed tomographic angiography (Figure 3C).

Discussion

In the present unblinded and uncontrolled pilot study, we documented that the transplantation of BM-MNCs was associated with an improvement in ischemic symptoms for up to 4 years. Indeed, VAS scores improved from 5.1±0.7 to 2.3±1.9 at follow-up. Furthermore, skin ulcers remained completely healed in 6 of 7 patients. In this regard, the present findings extend previous observations[11] by establishing the potential long-term benefit of BM-MNC transplantation for the treatment of arterial insufficiency.

It should be noted, however, that half of the patients suffered adverse events during follow-up. Such a high rate of adverse events cannot be explained by the natural course of the disease itself. In general, the prognosis of patients with thromboangiitis obliterans is directly related to tobacco

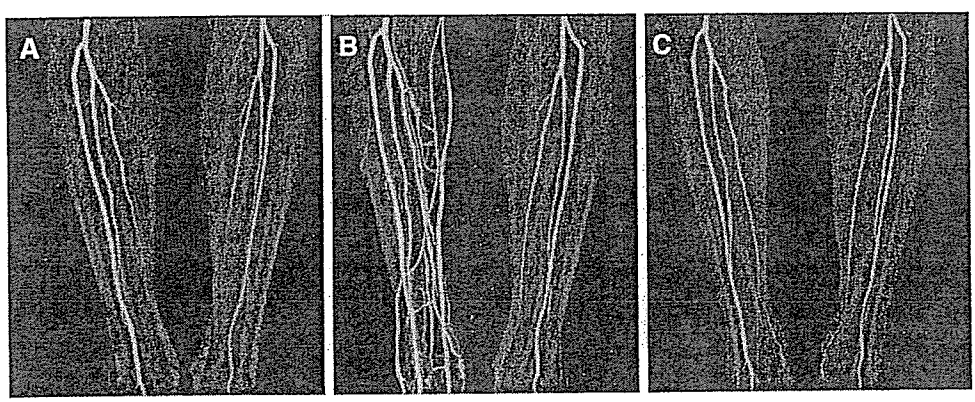

Figure 3. Computed tomographic angiography at (A) baseline, (B) 7 months, and (C) 1 year after cell transplantation. Early venous return of contrast material observed at 7 months spontaneously regressed by 1 year.

use.[12,13] Patients who are able to stop smoking avoid the recurrence of the disease and amputation.[14] In addition, unlike those with atherosclerosis of the extremities, these patients rarely show involvement of visceral vessels and do not appear to be at an increased risk of stroke or myocardial infarction. The mortality rates are thus not higher than those of age- and sex-matched populations.[15,16] It is entirely possible that the high rate of adverse events observed in our patients may have been directly related to BM-MNC transplantation rather than to the progression of the disease itself.

Patient 4 suddenly died at 20 months after transplantation at the age of 30 years. The deaths of patients receiving BM-MNC transplantation were previously reported in the TACT study, in which 2 of 25 patients died of acute myocardial infarction within 24 weeks after transplantation.[11] The patients' backgrounds in the TACT study, in terms of age and comorbidity, may have been totally different from those of our study, in which only patients with thromboangiitis obliterans were recruited. As mentioned above, in patients with thromboangiitis obliterans, coronary involvement is rare, and they usually do very well as long as they discontinue smoking.[12–16] Patient 4 had no risk factors for atherosclerosis and stopped smoking before BM-MNC transplantation. Furthermore, ^{201}thallium scintigraphy performed before transplantation documented no sign of myocardial ischemia. Considering the patient's background and the natural course of the disease,[12–16] the possibility that his death was related to BM-MNC transplantation cannot be excluded. In this regard, several studies have suggested the possible role of BM-MNCs in atherogenesis. A recent report by Silvestre et al,[17] for example, demonstrated that the transplantation of BM-MNCs into ischemic limbs of apolipoprotein E–knockout mice led to a significant increase in atherosclerotic plaque size at a distant site. More recently, George et al[18] have also shown that an intravenous injection of bone marrow cells into apolipoprotein E–knockout mice results in an increase in atherosclerotic lesion size, whereas an injection of endothelial progenitor cells influences plaque stability. These reports indicate that attempts to enhance neovascularization by using BM-MNCs could also enhance unwanted plaque growth and instability, thus suggesting the possibility that our young patient died of an acute coronary event due to accelerated atherogenesis after BM-MNC transplantation.

We also encountered the development of an arteriovenous shunt, which could be a potential consequence of BM-MNC transplantation. Indeed, concerns have been raised about the potential adverse effects of cell transplantation, ie, unregulated differentiation and proliferation. Wakitani et al[19] reported that teratoma formation could occur after embryonic stem cell transplantation. Yoon et al[20] documented intramyocardial calcification after the transplantation of bone marrow cells in rats. Our observations may provide another cautionary example of unregulated differentiation and proliferation. Although the arteriovenous shunt in our case was self-limited, it may represent unwanted angiogenesis; thus, careful monitoring is warranted for future patients who receive BM-MNC transplantation.

Worsening or recurrence of ischemic symptoms was observed in 3 patients. The short-term outcome at 1 month was poor in these patients except in the patient with an arteriovenous shunt. The improvement in rest pain was not substantial in 1 patient. Healing of the skin ulcer was incomplete in another. It is anticipated that a poor response 1 month after BM-MNC transplantation could result in a poor long-term outcome. It is important to note that, in the latter patient with incomplete healing of the skin ulcer, the angiographic improvement of the collateral network at 1 month remained unchanged at 5 months when worsening of the skin ulcer was observed. It is suggested that the temporal sequence of improvement in ischemic limb status does not necessarily parallel the temporal evolution of collateral development.

Conclusions

In this unblinded and uncontrolled pilot study, long-term adverse events after BM-MNC transplantation, including death and unfavorable angiogenesis, were observed in half of the patients with thromboangiitis obliterans. Given the current incomplete knowledge of the safety and efficacy of this strategy, careful long-term monitoring is required for future patients receiving BM-MNC transplantation.

Sources of Funding

This work was supported by Health and Labor Sciences Research Grants (H16-009, H16-017, H17-009), by Ministry of Health, Labor and Welfare Research Grants for Cardiovascular Disease (16C-6, 18C-4), and by grants from the New Energy and Industrial Technology Development Organization and the Japan Cardiovascular Research Foundation.

Disclosures

None.

References

1. Belch JJ, Topol EJ, Agnelli G. Critical issues in peripheral arterial disease detection and management: a call to action. *Arch Intern Med*. 2003;28: 884–892.
2. Dormandy JA, Rutherford RB. Management of peripheral artery disease (PAD). TASC Working Group. TransAtlantic InterSociety Consensus (TASC). *J Vasc Surg*. 2000;31:S1–S296.
3. Isner JM, Rosenfield K. Redefining the treatment of peripheral artery disease. *Circulation*. 1993;88:1534–1557.
4. Takeshita S, Zheng LP, Brogi E, Kearney M, Pu LO, Bunting S, Ferrara N, Symes JF, Isner JM. Therapeutic angiogenesis: a single intraarterial bolus of vascular endothelial growth factor augments revascularization in a rabbit ischemic hind limb model. *J Clin Invest*. 1994;93:662–670.
5. Isner J, Asahara T. Angiogenesis and vasculogenesis as therapeutic strategies for postnatal neovascularization. *J Clin Invest*. 1999;103: 1231–1236.
6. Asahara T, Murohara T, Sullivan A, Silver M, van der Zee R, Li T, Witzenbichler B, Schatteman G, Isner JM. Isolation of putative progenitor cells for angiogenesis. *Science*. 1997;275:964–967.
7. Asahara T, Masuda H, Takahashi T, Kalka C, Pastore C, Silver M, Kearney M, Magner M, Isner JM. Bone marrow origin of endothelial progenitor cells responsible for postnatal vasculogenesis in physiological and pathological neovascularization. *Circ Res*. 1999;85:221–228.
8. Shi Q, Rafii S, Wu M. Evidence for circulating bone marrow–derived endothelial cells. *Blood*. 1998;92:362–367.
9. Kalka C, Masuda H, Takahashi T, Kalka-Moll WM, Silver M, Kearney M, Li T, Isner JM, Asahara T. Transplantation of ex vivo expanded endothelial progenitor cells for therapeutic neovascularization. *Proc Natl Acad Sci U S A*. 2000;97:3423–3427.
10. Shintani S, Murohara T, Ikeda H, Ueno T, Sasaki K, Duan J, Imaizumi T. Augmentation of postnatal neovascularization with autologous bone marrow transplantation. *Circulation*. 2001;103:897–903.
11. Tateishi-Yuyama E, Matsubara H, Murohara T, Ikeda U, Shintani S, Masaki H, Amano K, Kishimoto Y, Yoshimoto K, Akashi H, Shimada K,

Iwasaka T, Imaizumi T. Therapeutic angiogenesis for patients with limb ischemia by autologous transplantation of bone marrow cells: a pilot study and a randomized controlled trial. *Lancet*. 2002;360:427–435.
12. Olin JW. Thromboangiitis obliterans (Buerger's disease). *N Engl J Med*. 2000;343:864–869.
13. Olin JW, Young JR, Graor RA, Ruschhaupt WF, Bartholomew JR. The changing clinical spectrum of thromboangiitis obliterans (Buerger's disease). *Circulation*. 1990;82(5 Suppl):IV3–IV8.
14. Matsushita M, Shionoya S, Matsumoto T. Urinary cotinine measurement in patients with Buerger's diseases: effects of active and passive smoking on the disease process. *J Vasc Surg*. 1991;14:53–58.
15. Szuba A, Cooke JP. Thromboangiitis obliterans: an update on Buerger's disease. *West J Med*. 1998;168:225–260.
16. Mills JL, Taylor LMJ, Porter JM. Buerger's disease in the modern era. *Am J Surg*. 1987;154:123–129.
17. Silvestre J-S, Gojova A, Brun V, Potteaux S, Esposito B, Duriez M, Clergue M, Le Ricousse-Roussanne S, Barateau V, Merval R, Groux H, Tobelem G, Levy B, Tedgui A, Mallat Z. Transplantation of bone marrow–derived mononuclear cells in ischemic apolipoprotein E–knockout mice accelerates atherosclerosis without altering plaque composition. *Circulation*. 2003;108:2839–2842.
18. George J, Afek A, Abashidze A, Shmilovich H, Deutsch V, Kopolovich J, Miller H, Keren G. Transfer of endothelial progenitor and bone marrow cells influences atherosclerotic plaque size and composition in apolipoprotein E knockout mice. *Arterioscler Thromb Vasc Biol*. 2005;25:2636–2641.
19. Wakitani S, Takaoka K, Hattori T, Miyazawa N, Iwanaga T, Takeda S, Watanabe TK, Tanigami A. Embryonic stem cells injected into the mouse knee joint form teratomas and subsequently destroy the joint. *Rheumatology (Oxford)*. 2003;42:162–165.
20. Yoon Y, Park J, Tkebuchava T, Luedeman C, Losordo D. Unexpected severe calcification after transplantation of bone marrow cells in acute myocardial infarction. *Circulation*. 2004;109:3154–3157.

CLINICAL PERSPECTIVE

The favorable short-term outcome of bone marrow mononuclear cell transplantation (BM-MNC) transplantation has been established in patients with critical limb ischemia. However, the long-term outcome of this treatment strategy has not been determined yet. In our case series, we documented that long-term adverse events, including death and unfavorable angiogenesis, were observed in 4 of 8 patients receiving BM-MNC transplantation. The first patient suffered sudden death at 20 months after transplantation at 30 years of age. The second patient with incomplete healing of a skin ulcer showed worsening of the lesion at 4 months. The third patient had worsening of rest pain at 8 months. The last patient developed an arteriovenous shunt in the foot at 7 months, which spontaneously regressed by 1 year. Given the current incomplete knowledge on the safety and efficacy of this strategy, it is suggested that careful long-term monitoring is required in patients receiving BM-MNC transplantation. To our knowledge, this is the first report on the long-term outcome of transplantation of BM-MNCs for critical limb ischemia, and the first that documents the development of unfavorable angiogenesis and sudden death after therapeutic angiogenesis.

Japanese Journal of Applied Physics
Vol. 45, No. 6A, 2006, pp. 5301–5306

X-ray Spectra from Weakly Ionized Linear Copper Plasma

Eiichi SATO, Yasuomi HAYASHI, Rudolf GERMER[1], Etsuro TANAKA[2], Hidezo MORI[3], Toshiaki KAWAI[4], Takashi INOUE[5], Akira OGAWA[5], Shigehiro SATO[6], Kazuyoshi TAKAYAMA[7] and Jun ONAGAWA[8]

Department of Physics, Iwate Medical University, 3-16-1 Honchodori, Morioka 020-0015, Japan
[1]*ITP, FHTW FB1 and TU-Berlin, Blankenhainer Str. 9, D 12249 Berlin, Germany*
[2]*Department of Nutritional Science, Faculty of Applied Bio-science, Tokyo University of Agriculture, 1-1-1 Sakuragaoka, Setagaya-ku, Tokyo 156-8502, Japan*
[3]*Department of Cardiac Physiology, National Cardiovascular Center Research Institute, 5-7-1 Fujishirodai, Suita, Osaka 565-8565, Japan*
[4]*Electron Tube Division #2, Hamamatsu Photonics K.K., 314-5 Shimokanzo, Iwata, Shizuoka 438-0193, Japan*
[5]*Department of Neurosurgery, School of Medicine, Iwate Medical University, 19-1 Uchimaru, Morioka 020-8505, Japan*
[6]*Department of Microbiology, School of Medicine, Iwate Medical University, 19-1 Uchimaru, Morioka 020-8505, Japan*
[7]*Shock Wave Research Center, Institute of Fluid Science, Tohoku University, 2-1-1 Katahira, Sendai 980-8577, Japan*
[8]*Department of Applied Physics and Informatics, Faculty of Engineering, Tohoku Gakuin University, 1-13-1 Chuo, Tagajo, Miyagi 985-8537, Japan*

(Received November 20, 2005; accepted April 5, 2006; published online June 8, 2006)

In the plasma flash X-ray generator, a 200 nF condenser is charged up to 50 kV by a power supply, and flash X-rays are produced by the discharging. The X-ray tube is a demountable triode with a trigger electrode, and the turbomolecular pump evacuates air from the tube with a pressure of approximately 1 mPa. Target evaporation leads to the formation of weakly ionized linear plasma, consisting of copper ions and electrons, around the fine target, and intense Kα lines are left using a 10-μm-thick nickel filter. At a charging voltage of 50 kV, the maximum tube voltage was almost equal to the charging voltage of the main condenser, and the peak current was about 16 kA. The K-series characteristic X-rays were clean and intense, and higher harmonic X-rays were observed. The X-ray pulse widths were approximately 300 ns, and the time-integrated X-ray intensity had a value of approximately 1.5 mGy per pulse at 1.0 m from the X-ray source with a charging voltage of 50 kV. [DOI: 10.1143/JJAP.45.5301]

KEYWORDS: linear plasma, X-ray spectra, K-series characteristic X-rays, bremsstrahlung X-rays, higher harmonic X-rays

1. Introduction

In order to produce X-ray lasers, several different methods have been developed, and a discharge capillary[1–3] is very useful to increase the laser pulse energy with increases in the capillary length. However, it is difficult to increase the laser photon energy to 10 keV or beyond.

Using monochrocollimators, synchrotrons produce monochromatic parallel beams, which are fairly similar to monochromatic parallel laser beams, and the beams have been applied to various research project including phase-contrast radiography[4,5] and enhanced K-edge angiography.[6,7] Because there are no X-ray resonators in the high-photon-energy region, new methods for increasing coherence will be desired in the future.

To apply flash X-ray generators to biomedicine, several different generators[8–13] have been developed, and plasma X-ray generators[14–17] are useful for producing clean characteristic X-rays in the low-photon-energy region of less than 10 keV. By forming weakly ionized linear plasma using rod targets, intense K-series characteristic X-rays are observed from the axial direction of the linear plasmas of nickel and copper, since the bremsstrahlung X-rays are absorbed effectively by the linear plasma. We are therefore very interested in the X-ray spectra produced by increasing the charging voltage in the high photon energy region beyond Kβ energies.

In this paper, we describe a recent table-top plasma flash X-ray generator utilizing a rod target triode, used to perform a preliminary experiment for generating clean K-series characteristic X-rays and their higher harmonic hard X-rays by forming a linear copper plasma cloud around a fine target.

2. Generator

Figure 1 shows a block diagram of the high-intensity plasma flash X-ray generator. This generator consists of the following essential components: a high-voltage power supply, a high-voltage condenser with a capacity of approximately 200 nF, a turbomolecular pump, a krytron pulse generator as a trigger device, and a flash X-ray tube. The high-voltage main condenser is charged to 50 kV by the power supply, and electric charges in the condenser are discharged to the tube after triggering the cathode electrode with the trigger device. The plasma flash X-rays are then produced.

The X-ray tube is a demountable cold-cathode triode that is connected to the turbomolecular pump with a pressure of approximately 1 mPa. This tube consists of the following major parts: a hollow cylindrical carbon cathode with a bore diameter of 10.0 mm, a brass focusing electrode, a trigger electrode made from copper wire, a stainless steel vacuum chamber, a nylon insulator, a poly(ethylene terephthalate) (Mylar) X-ray window 0.25 mm in thickness, and a rod-shaped copper target 3.0 mm in diameter with a tip angle of 60°. The distance between the target and cathode electrodes is approximately 20 mm, and the trigger electrode is set in the cathode electrode. As electron beams from the cathode electrode are roughly converged to the target by the focusing electrode, evaporation leads to the formation of a weakly ionized linear plasma,[18] consisting of copper ions and electrons, around the fine target.

In the linear plasma, bremsstrahlung photons with energies higher than the K-absorption edge are effectively absorbed and are converted into fluorescent X-rays. The plasma then transmits the fluorescent rays easily, and bremsstrahlung rays with energies lower than the K-edge

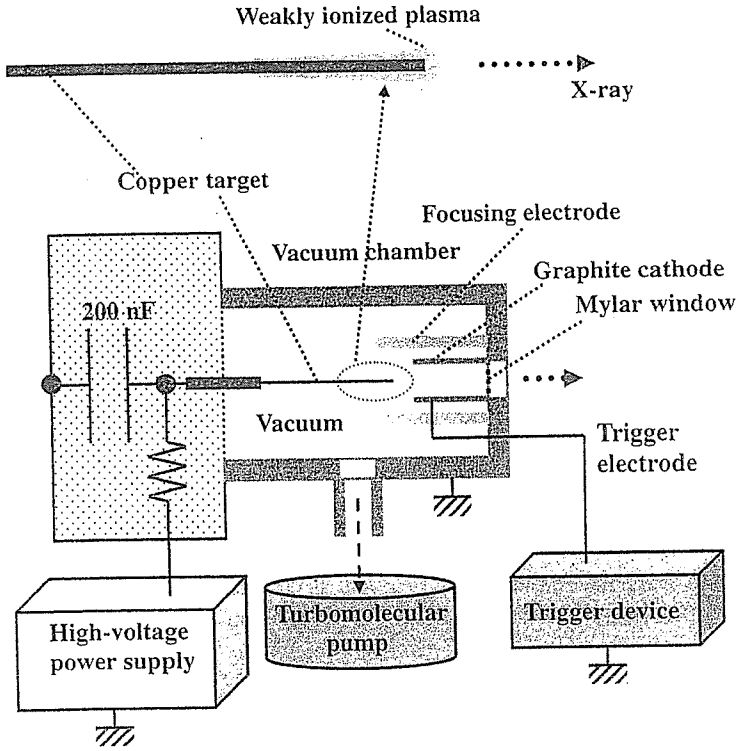

Fig. 1. Block diagram including the electric circuit of the plasma flash X-ray generator.

are also absorbed by the plasma. In addition, because bremsstrahlung rays are not emitted in the opposite direction to that of electron trajectory, intense characteristic X-rays are generated from the plasma-axial direction.

3. Characteristics

3.1 Tube voltage and current

Tube voltage and current were measured by a high-voltage divider with an input impedance of 1 GΩ and a current transformer, respectively. The withstand voltage of the divider is approximately 60 kV, and the measurable current of the transformer ranges from 1 A to 100 kA. Figure 2 shows the time relation between the tube voltage and current. At the indicated charging voltages, they roughly displayed damped oscillations. When the charging voltage was increased, both the maximum tube voltage and current increased. At a charging voltage of 50 kV, the maximum tube voltage was almost equal to the charging voltage of the main condenser, and the maximum tube current was approximately 16 kA.

3.2 X-ray output

X-ray output pulse was detected using a combination of a plastic scintillator and a photomultiplier (Fig. 3). The X-ray pulse height substantially increased with corresponding increases in the charging voltage. The rise time increased with increasing the voltage because the K-series characteristic X-rays were produced with tube voltages beyond the critical excitation voltage of 8.9 kV. The X-ray pulse widths were about 300 ns, and the time-integrated X-ray intensity per pulse measured by a thermoluminescence dosimeter (Kyokko TLD Reader 1500 having MSO-S elements without energy compensation) had a value of approximately 1.5 mGy at 1.0 m from the X-ray source with a charging voltage of 50 kV. The TLD reader has a wide measurable range of from 1 μSv to 100 Sv.

3.3 X-ray source

In order to roughly observe images of the plasma X-ray source in the detector plane, we employed a pinhole camera with a hole diameter of 100 μm without using a filter (Fig. 4). When the charging voltage was increased, the plasma X-ray source grew, and both spot dimension and intensity increased. Because the X-ray intensity is the highest at the center of the spot, both the dimension and intensity decreased according to both increases in the thickness of a filter for absorbing X-rays and decreases in the pinhole diameter.

3.4 X-ray spectra

X-ray spectra from the plasma source were measured by a transmission-type spectrometer with a lithium fluoride curved crystal 0.5 mm in thickness. The spectra were taken by a computed radiography (CR) system[19] (Konica Minolta, Regius 150) with a wide dynamic range beyond five figures for measuring X-ray intensity, and relative X-ray intensity was calculated from Dicom digital data. Subsequently, the relative X-ray intensity as a function of the data was calibrated using a conventional X-ray generator, and we confirmed that the intensity was proportional to the exposure time. Figure 5 shows measured spectra from the copper target at the indicated conditions. In fact, we observed clean K lines, and Kα lines were left by absorbing Kβ lines using a 10-μm-thick nickel filter. When the charging voltage was increased, the characteristic X-ray intensity substantially increased. In particular, we confirmed the irradiation of

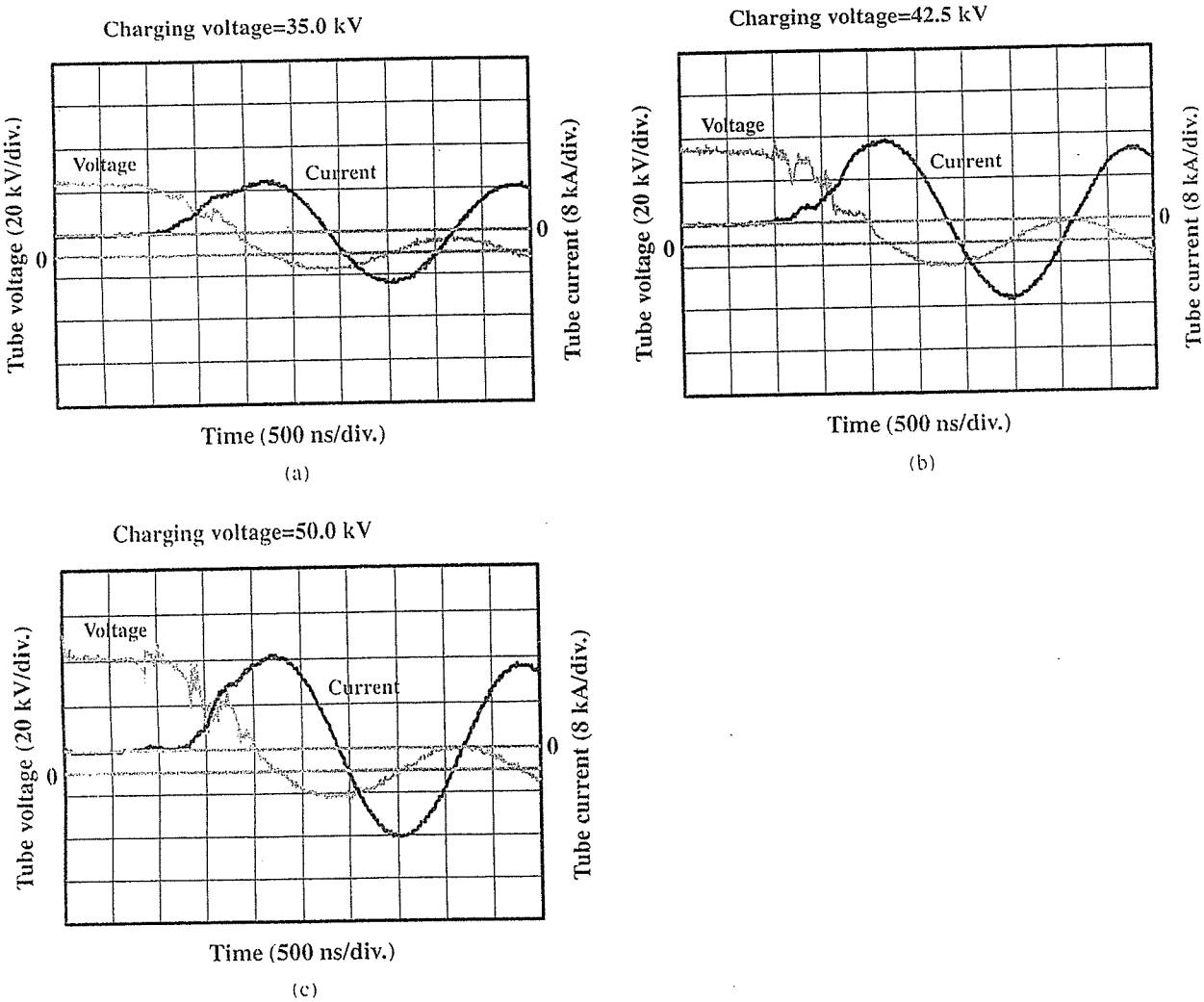

Fig. 2. Tube voltages and currents with a charging voltage of (a) 35.0, (b) 42.5, and (b) 50.0 kV.

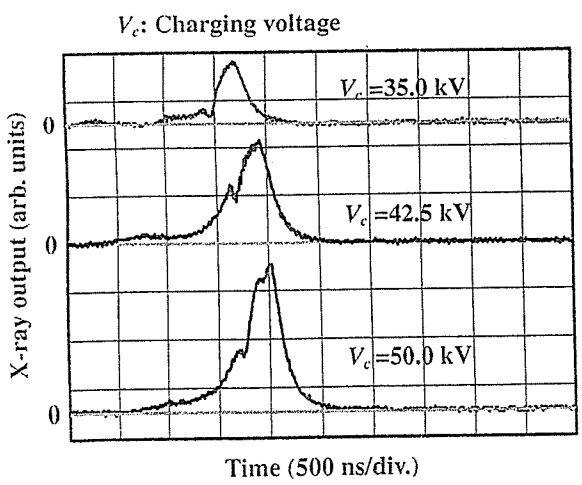

Fig. 3. X-ray outputs at the indicated conditions.

the second and fourth harmonic X-rays of the fundamental K-series characteristic X-rays from copper target. The X-ray intensities of the harmonics increased with increases in the charging voltage, and the harmonic bremsstrahlung rays survived due to the X-ray resonation in the plasma.

4. Radiography

The plasma radiography was performed by the CR system using the filter. The charging voltage and the distance between the X-ray source and imaging plate were 50 kV and 1.2 m, respectively. First, rough measurements of spatial resolution were made using wires. Figure 6 shows radiograms of tungsten wires coiled around pipes made of poly(methyl methacrylate) (PMMA). Although the image contrast decreased somewhat with decreases in the wire diameter, due to blurring of the image caused by the sampling pitch of 87.5 μm, a 50-μm-diameter wire could be observed.

Figure 7 shows a radiogram of plastic bullets falling into a polypropylene beaker from a plastic test tube. Because the X-ray duration was about 0.5 μs, the stop-motion image of bullets could be obtained. Next, a radiogram of a vertebra is shown in Fig. 8, and fine structures in the vertebra were observed. Finally, Fig. 9 shows an angiogram of a rabbit ear; iodine-based microspheres of 15 μm in diameter were used, and fine blood vessels of about 100 μm were visible.

5. Conclusions and Outlook

We obtained fairly intense and clean K lines from a weakly ionized linear copper plasma, and Kα lines were left

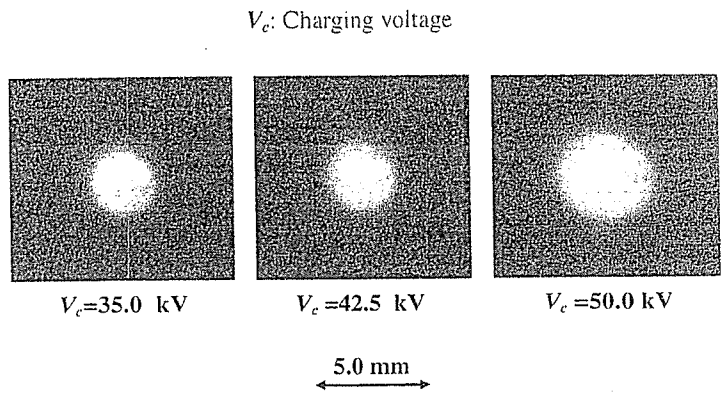

Fig. 4. Images of the plasma X-ray source.

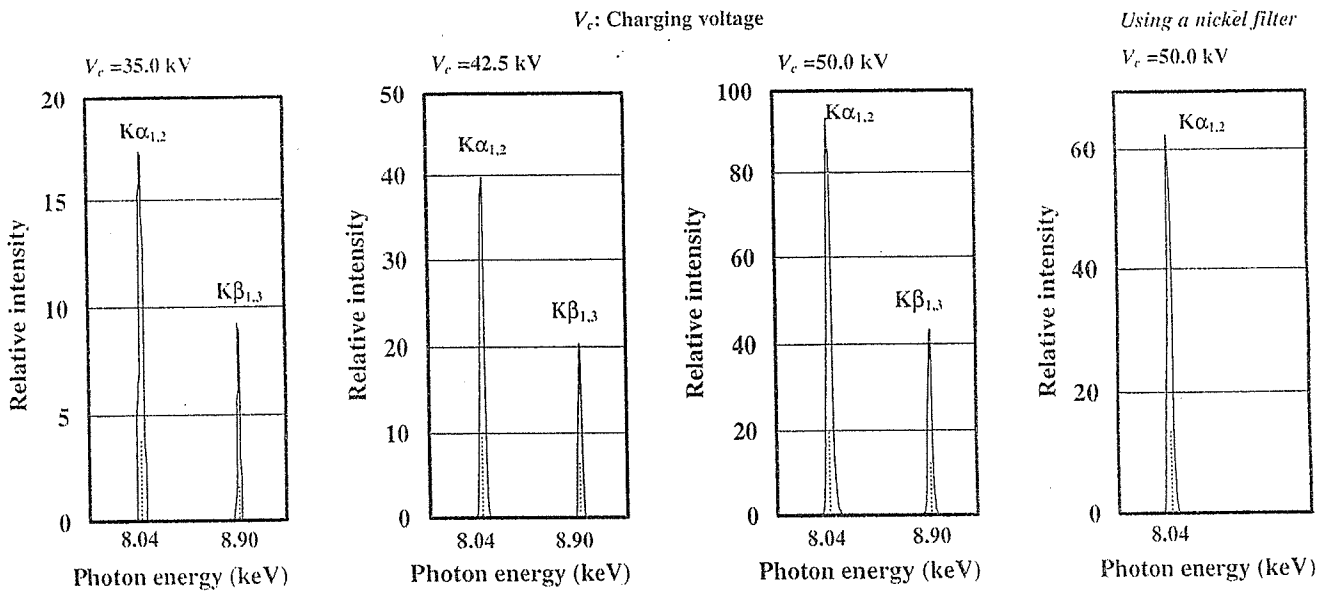

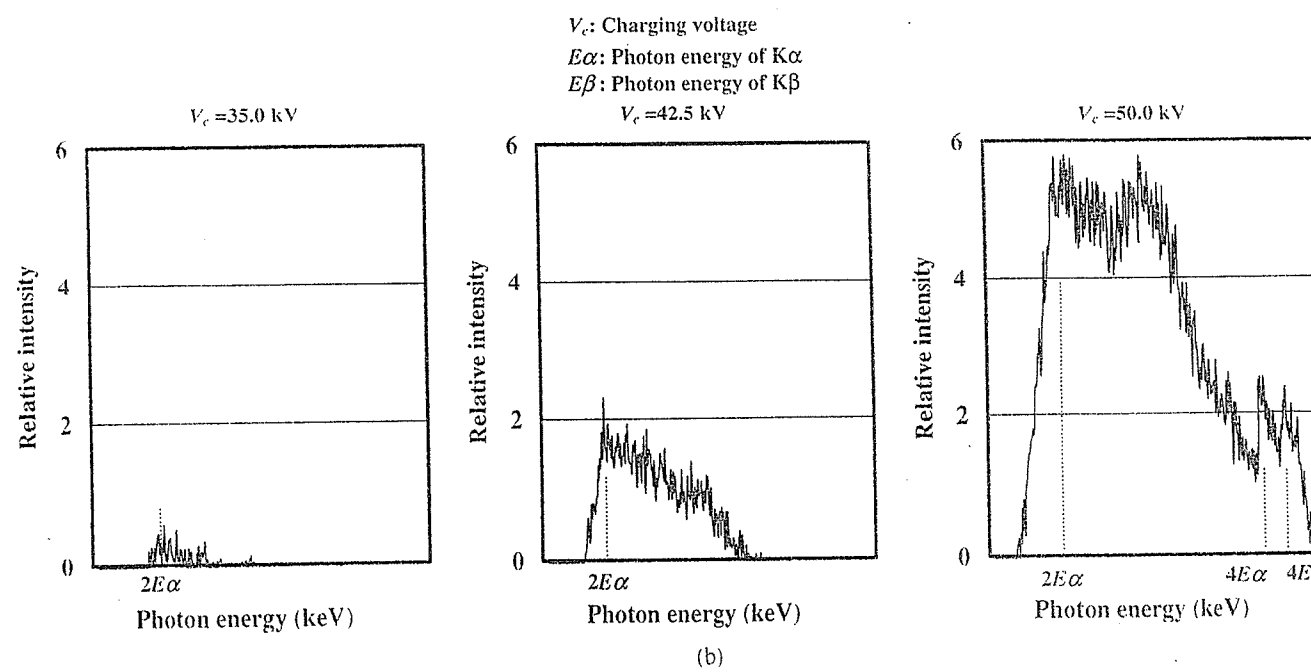

Fig. 5. X-ray spectra from weakly ionized copper plasma at the indicated conditions. (a) characteristic X-rays and (b) higher harmonic X-rays.

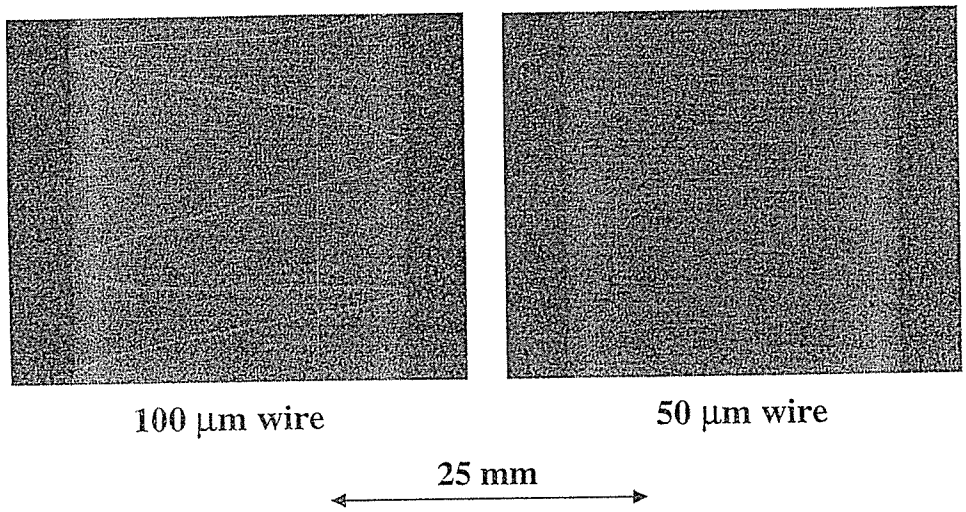

Fig. 6. Radiograms of tungsten wires coiled around PMMA pipes.

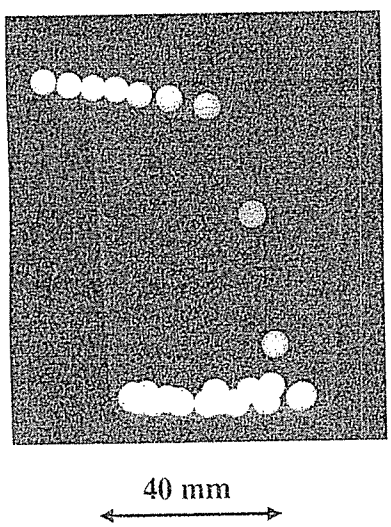

Fig. 7. Radiogram of plastic bullets falling into polypropylene beaker from a plastic test tube.

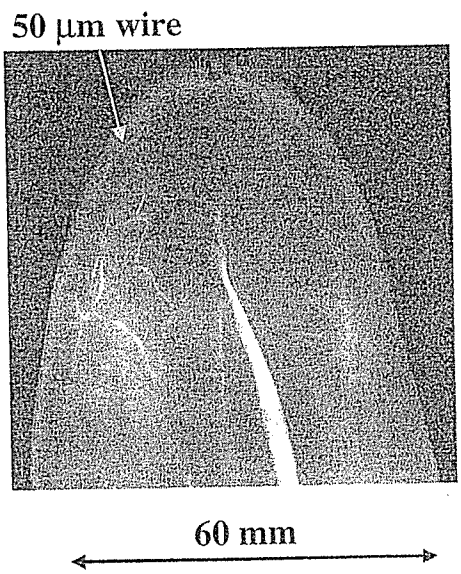

Fig. 9. Angiogram of a rabbit ear.

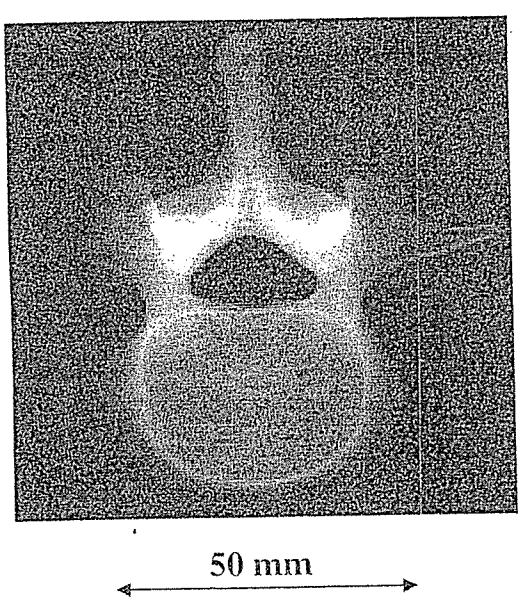

Fig. 8. Radiogram of a vertebra.

by the nickel filter. Both the characteristic and the harmonic X-ray intensities substantially increased with increasing the charging voltage.

In cases where weakly ionized linear plasma is employed, intense and clean K-series characteristic X-rays can be obtained. However, it is not easy to produce high-photon-energy K-series characteristic X-rays because the linear plasma transmits high-photon-energy bremsstrahlung X-rays; the effective thickness of a monochromatic metal filter increases with increases in the atomic number. Therefore, high-photon-energy plasma flash X-ray generators utilizing the angle dependence of bremsstrahlung X-rays are very useful to produce K photons of molybdenum, silver, cerium, tantalum, and tungsten. In particular, Kα rays of tantalum and tungsten are useful for performing enhanced K-edge angiography using gadolinium contrast media, and cerium K rays can be employed to perform iodine K-edge angiography.

In this research, we obtained sufficient characteristic X-ray intensity per pulse for CR radiography, and the

generator produced number of characteristic K photons was approximately 1×10^8 photons/cm^2 at 1.0 m per pulse. In addition, we are very interested in producing steady-state clean K rays and their higher harmonic hard X-rays using a similar tube.

Acknowledgments

This work was supported by Grants-in-Aid for Scientific Research (13470154, 13877114, 16591181, and 16591222) and Advanced Medical Scientific Research from MECSST, Health and Labor Sciences Research Grants (RAMT-nano-001, RHGTEFB-genome-005 and RHGTEFB-saisei-003), Grants from The Keiryo Research Foundation, The Promotion and Mutual Aid Corporation for Private Schools of Japan, Japan Science and Technology Agency (JST), and the New Energy and Industrial Technology Development Organization (NEDO, Industrial Technology Research Grant Program in '03).

1) J. J. Rocca, V. Shlyaptsev, F. G. Tomasel, O. D. Cortazar, D. Hartshorn and J. L. A. Chilla: Phys. Rev. Lett. **73** (1994) 2192.
2) C. D. Macchietto, B. R. Benware and J. J. Rocca: Opt. Lett. **24** (1999) 1115.
3) J. J. G. Rocca, J. L. A. Chilla, S. Sakadzic, A. Rahman, J. Filevich, E. Jankowska, E. C. Hammarsten, B. M. Luther, H. C. Kapteyn, M. Murnane and V. N. Shlyapsev: Proc. SPIE **4505** (2001) 1.
4) A. Momose, T. Takeda, Y. Itai and K. Hirano: Nat. Med. **2** (1996) 473.
5) M. Ando, A. Maksimenko, H. Sugiyama, W. Pattanasiriwisawa, K. Hyodo and C. Uyama: Jpn. J. Appl. Phys. **41** (2002) L1016.
6) H. Mori *et al.*: Radiology **201** (1996) 173.
7) K. Hyodo, M. Ando, Y. Oku, S. Yamamoto, T. Takeda, Y. Itai, S. Ohtsuka, Y. Sugishita and J. Tada: J. Synchrotron Radiat. **5** (1998) 1123.
8) E. Sato, S. Kimura, S. Kawasaki, H. Isobe, K. Takahashi, Y. Tamakawa and T. Yanagisawa: Rev. Sci. Instrum. **61** (1990) 2343.
9) K. Takahashi, E. Sato, M. Sagae, T. Oizumi, Y. Tamakawa and T. Yanagisawa: Jpn. J. Appl. Phys. **33** (1994) 4146.
10) E. Sato, K. Takahashi, M. Sagae, S. Kimura, T. Oizumi, Y. Hayasi, Y. Tamakawa and T. Yanagisawa: Med. Biol. Eng. Comput. **32** (1994) 289.
11) E. Sato, M. Sagae, K. Takahashi, A. Shikoda, T. Oizumi, Y. Hayasi, Y. Tamakawa and T. Yanagisawa: Med. Biol. Eng. Comput. **32** (1994) 295.
12) E. Sato, M. Sagae, E. Tanaka, Y. Hayasi, R. Germer, H. Mori, T. Kawai, T. Ichimaru, S. Sato, K. Takayama and H. Ido: Jpn. J. Appl. Phys. **43** (2004) 7324.
13) E. Sato, E. Tanaka, H. Mori, T. Kawai, T. Ichimaru, S. Sato, K. Takayama and H. Ido: Med. Phys. **32** (2005) 49.
14) E. Sato, Y. Hayasi, R. Germer, E. Tanaka, H. Mori, T. Kawai, H. Obara, T. Ichimaru, K. Takayama and H. Ido: Jpn. J. Med. Phys. **23** (2003) 123.
15) E. Sato, Y. Hayasi, R. Germer, E. Tanaka, H. Mori, T. Kawai, T. Ichimaru, K. Takayama and H. Ido: Rev. Sci. Instrum. **74** (2003) 5236.
16) E. Sato, Y. Hayasi, R. Germer, E. Tanaka, H. Mori, T. Kawai, T. Ichimaru, S. Sato, K. Takayama and H. Ido: J. Electron Spectrosc. Relat. Phenom. C **137–140** (2004) 713.
17) E. Sato, E. Tanaka, H. Mori, T. Kawai, S. Sato and K. Takayama: Opt. Eng. **44** (2005) 049002.
18) E. Sato, M. Sagae, K. Takahashi, T. Ichimaru, W. Aiba, S. Kumagai, Y. Hayasi, H. Ido, K. Sakamaki, K. Takayama and Y. Tamakawa: Proc. SPIE **3336** (1998) 75.
19) E. Sato, K. Sato and Y. Tamakawa: Ann. Rep. Iwate Med. Univ. Sch. Lib. Arts Sci. **35** (2000) 13.

Available online at www.sciencedirect.com
ScienceDirect
Radiation Physics and Chemistry 75 (2006) 1812–1818
Radiation Physics and Chemistry
www.elsevier.com/locate/radphyschem

Preliminary study for producing higher harmonic hard X-rays from weakly ionized nickel plasma

Eiichi Sato[a,*], Yasuomi Hayasi[a], Etsuro Tanaka[b], Hidezo Mori[c], Toshiaki Kawai[d], Takashi Inoue[e], Akira Ogawa[e], Shigehiro Sato[f], Kazuyoshi Takayama[g], Jun Onagawa[h], Hideaki Ido[h]

[a]*Department of Physics, Iwate Medical University, 3-16-1 Honchodori, Morioka 020-0015, Japan*
[b]*Department of Nutritional Science, Faculty of Applied Bio-science, Tokyo University of Agriculture, 1-1-1 Sakuragaoka, Setagaya-ku 156-8502, Japan*
[c]*Department of Cardiac Physiology, National Cardiovascular Center Research Institute, 5-7-1 Fujishirodai, Suita, Osaka 565-8565, Japan*
[d]*Electron Tube Division #2, Hamamatsu Photonics K. K., 314-5 Shimokanzo, Iwata 438-0193, Japan*
[e]*Department of Neurosurgery, School of Medicine, Iwate Medical Universichimaru, Morioka 020-8505, Japan*
[f]*Department of Microbiology, School of Medicine, Iwate Medical University, 19-1 Uchimaru, Morioka 020-8505, Japan*
[g]*Shock Wave Research Center, Institute of Fluid Science, Tohoku University, 2-1-1 Katahira, Sendai 980-8577, Japan*
[h]*Department of Applied Physics and Informatics, Faculty of Engineering, Tohoku Gakuin University, 1-13-1 Chuo, Tagajo 985-8537, Japan*

Accepted 23 November 2005

Abstract

In the plasma flash X-ray generator, a 200 nF condenser is charged up to 50 kV by a power supply, and flash X-rays are produced by the discharging. The X-ray tube is a demountable triode with a trigger electrode, and the turbomolecular pump evacuates air from the tube with a pressure of approximately 1 mPa. Target evaporation leads to the formation of weakly ionized linear plasma, consisting of nickel ions and electrons, around the fine target, and intense Kα lines are left using a 15-μm-thick cobalt filter. At a charging voltage of 50 kV, the maximum tube voltage was almost equal to the charging voltage of the main condenser, and the peak current was about 18 kA. The K-series characteristic X-rays were clean and intense, and higher harmonic X-rays were observed. The X-ray pulse widths were approximately 300 ns, and the time-integrated X-ray intensity had a value of approximately 1.0 mGy at 1.0 m from the X-ray source with a charging voltage of 50 kV.

PACS: 52.80.Vp; 52.90.+z; 87.59.Bh; 87.64.Gb

Keywords: Weakly ionized linear plasma; K-series characteristic X-rays; Clean characteristic X-rays; Higher harmonic hard X-rays

1. Introduction

In conjunction with single crystals, synchrotrons produce monochromatic parallel beams, which are fairly similar to monochromatic parallel laser beams, and the

*Corresponding author.
E-mail address: dresato@iwate-med.ac.jp (E. Sato).

0969-806X/$ - see front matter © 2006 Elsevier Ltd. All rights reserved.
doi:10.1016/j.radphyschem.2005.11.012

beams have been applied to enhanced K-edge angiography (Thompson et al., 1992; Mori et al., 1996; Hyodo et al., 1998), phase-contrast radiography (Davis et al., 1995; Momose et al., 1996; Ando et al., 2002), and crystallography. Therefore, the production of coherent hard X-ray lasers for various research projects, including biomedical applications, has long been wished for.

Recently, soft X-ray lasers have been produced by a gas-discharge capillary (Rocca et al., 1994, 1996; Macchietto et al., 1999), and the laser pulse energy substantially increased in proportion to the capillary length. These kinds of fast discharges can generate hot and dense plasma columns with aspect ratios approaching 1000:1. However, it is difficult to increase the laser photon energy to 10 keV or beyond. Because there are no X-ray resonators in the high-photon-energy region, new methods for increasing coherence will be desired in the future.

To apply flash X-ray generators to biomedicine, several different generators have been developed (Germer, 1979; Sato et al., 1990, 1994a, b; Shikoda et al., 1994; Takahashi et al., 1994), and plasma X-ray generators (Sato et al., 2003a, b, 2004a–c, 2005a–c) are useful for producing clean characteristic X-rays in the low-photon-energy region of less than 20 keV. By forming weakly ionized linear plasma using rod targets, we confirmed irradiation of intense K-series characteristic X-rays from the axial direction of the linear plasmas of nickel, copper, and molybdenum, since the bremsstrahlung X-rays are absorbed effectively by the linear plasma; monochromatic clean Kα rays were produced using K-edge filters.

In this paper, we describe a recent plasma flash X-ray generator utilizing a rod target, used to perform a preliminary experiment for generating clean K-series characteristic X-rays and their higher harmonic hard X-rays by forming a plasma cloud around a fine target.

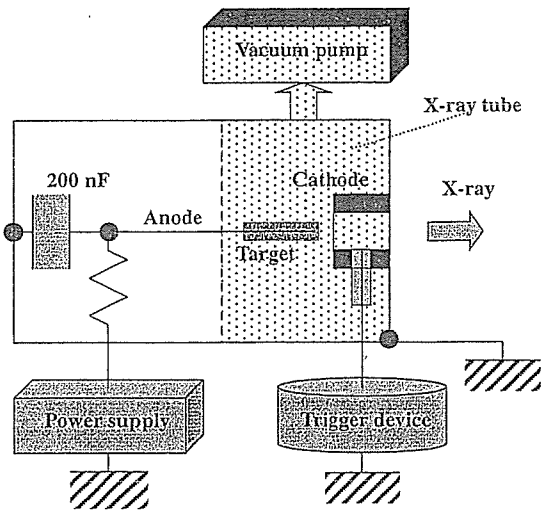

Fig. 1. Block diagram including electric circuit of the plasma flash X-ray generator.

2. Generator

Fig. 1 shows a block diagram of the high-intensity plasma flash X-ray generator. This generator consists of the following essential components: a high-voltage power supply, a high-voltage condenser with a capacity of approximately 200 nF, a turbomolecular pump, a krytron pulse generator as a trigger device, and a flash X-ray tube. The high-voltage main condenser is charged to 50 kV by the power supply, and electric charges in the condenser are discharged to the tube after triggering the cathode electrode with the trigger device. The plasma flash X-rays are then produced.

The schematic drawing of the plasma X-ray tube is illustrated in Fig. 2. The X-ray tube is a demountable

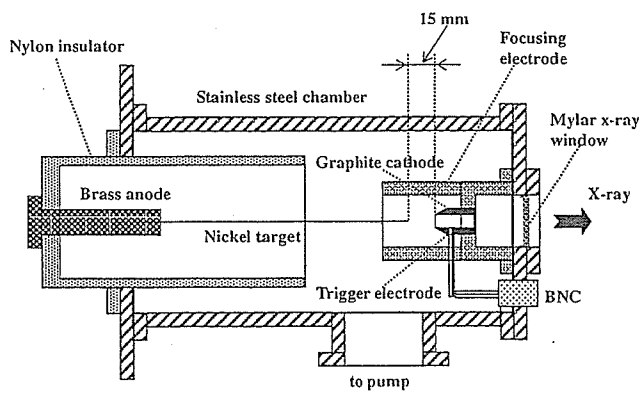

Fig. 2. Schematic drawing of the flash X-ray tube with a rod nickel target.

cold-cathode triode that is connected to the turbomolecular pump with a pressure of approximately 1 mPa. This tube consists of the following major parts: a hollow cylindrical carbon cathode with a bore diameter of 10.0 mm, a brass focusing electrode, a trigger electrode made from copper wire, a stainless steel vacuum chamber, a nylon insulator, a polyethylene terephthalate (Mylar) X-ray window 0.25 mm in thickness, and a rod-shaped nickel target 3.0 mm in diameter with a tip angle of 60°. The distance between the target and cathode electrodes is approximately 15 mm, and the trigger electrode is set in the cathode electrode. As electron beams from the cathode electrode are roughly converged to the target by the focusing electrode, evaporation leads to the formation of a weakly ionized linear plasma, consisting of nickel ions and electrons, around the fine target.

In the linear plasma, bremsstrahlung photons with energies higher than the K-absorption edge are effectively absorbed and are converted into fluorescent X-rays. The plasma then transmits the fluorescent rays easily, and bremsstrahlung rays with energies lower than the K-edge are also absorbed by the plasma. In addition, because bremsstrahlung rays are not emitted in the opposite direction to that of electron trajectory, intense characteristic X-rays are generated from the plasma-axial direction.

3. Characteristics

3.1. Tube voltage and current

Tube voltage and current were measured by a high-voltage divider with an input impedance of 1 GΩ and a current transformer, respectively. Fig. 3 shows the time relation between the tube voltage and current. At the indicated charging voltages, they roughly displayed damped oscillations. When the charging voltage was increased, both the maximum tube voltage and current increased. At a charging voltage of 50 kV, the maximum tube voltage was almost equal to the charging voltage of the main condenser, and the maximum tube current was approximately 18 kA.

3.2. X-ray output

X-ray output pulse was detected using a combination of a plastic scintillator and a photomultiplier (Fig. 4). The X-ray pulse height substantially increased with corresponding increases in the charging voltage. The X-ray pulse widths were about 300 ns, and the time-integrated X-ray intensity measured by a thermoluminescence dosimeter (Kyokko TLD Reader 1500 having MSO-S elements without energy compensation) had a value of about 1.0 mGy at 1.0 m from the X-ray source with a charging voltage of 50 kV.

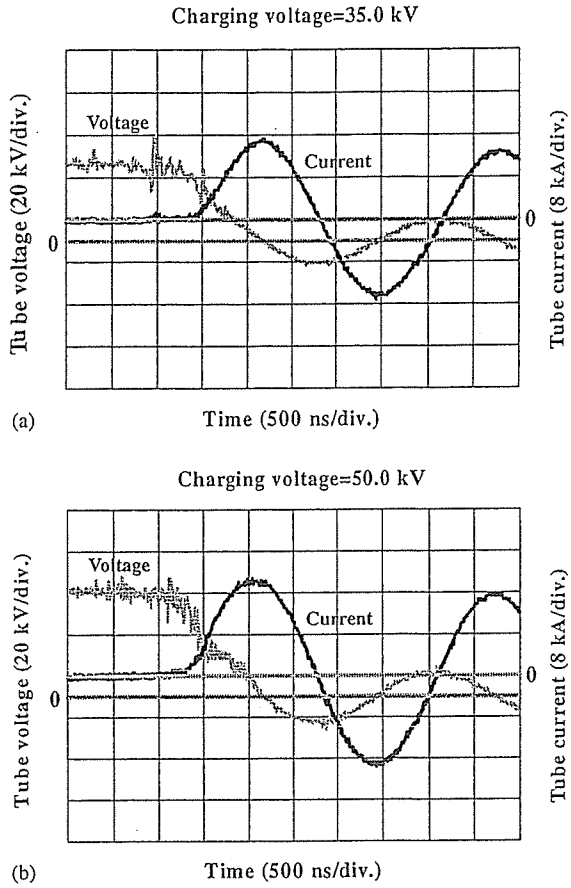

Fig. 3. Tube voltages and currents with a charging voltage of (a) 35.0 kV and (b) 50.0 kV.

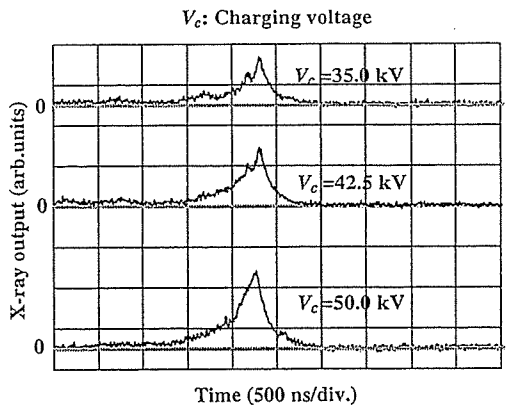

Fig. 4. X-ray outputs at the indicated conditions.

3.3. X-ray source

In order to roughly observe images of the plasma X-ray source in the detector plane, we employed a pinhole camera with a hole diameter of 100 μm (Fig. 5). When

the charging voltage was increased, the plasma X-ray source grew, and both spot dimension and intensity increased. Because the X-ray intensity is the highest at the center of the spot, both the dimension and intensity decreased according to both increases in the thickness of a filter for absorbing X-rays and decreases in the pinhole diameter.

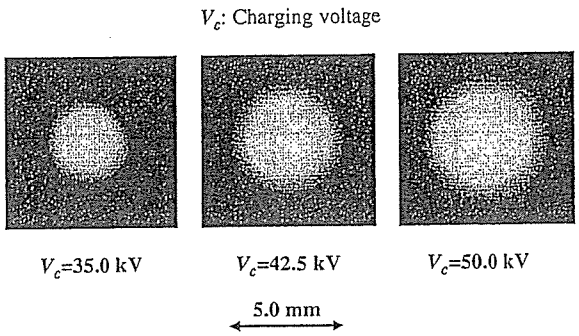

Fig. 5. Images of plasma X-ray source.

3.4. X-ray spectra

X-ray spectra from the plasma source were measured by a transmission-type spectrometer with a lithium fluoride curved crystal 0.5 mm in thickness. The spectra were taken by a computed radiography (CR) system (Sato et al., 2000) (Konica Minolta Regius 150) with a wide dynamic range, and relative X-ray intensity was calculated from Dicom digital data. Subsequently, the relative X-ray intensity as a function of the data was calibrated using a conventional X-ray generator, and we confirmed that the intensity was proportional to the

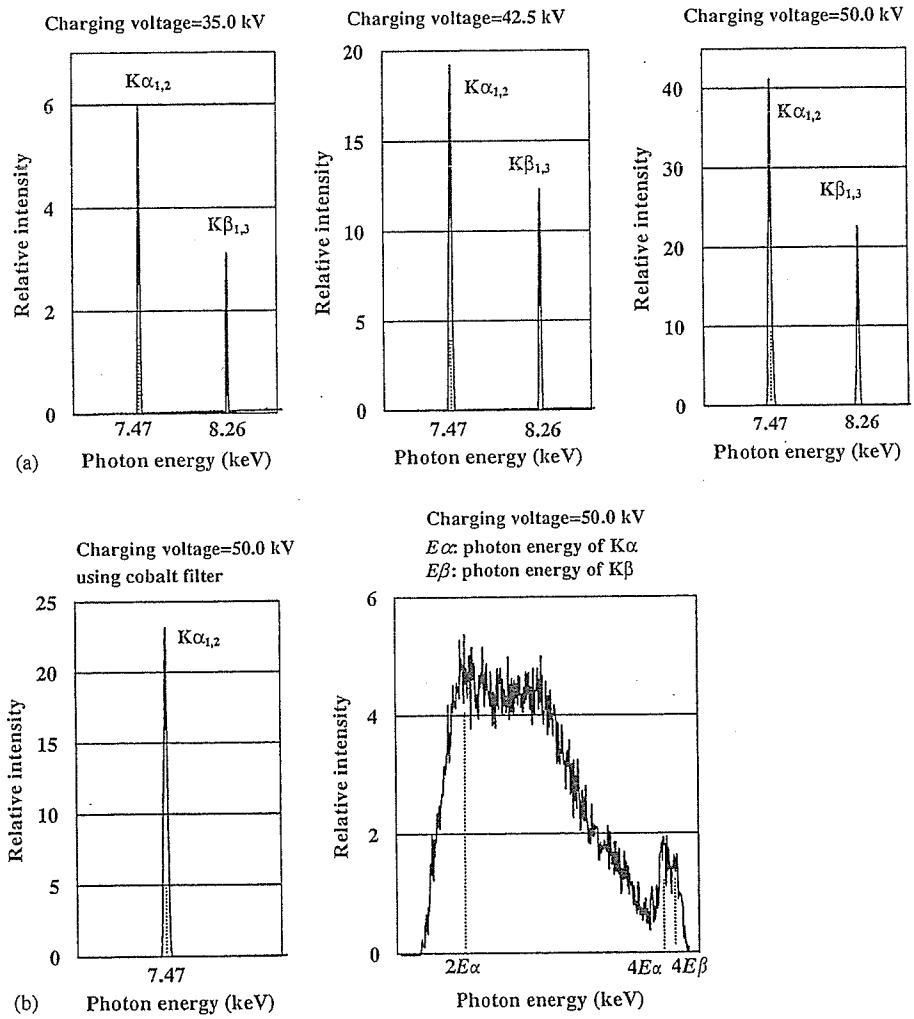

Fig. 6. X-ray spectra from weakly ionized nickel plasma at the indicated conditions. (a) Kα and Kβ rays and (b) Kα and higher harmonic rays.

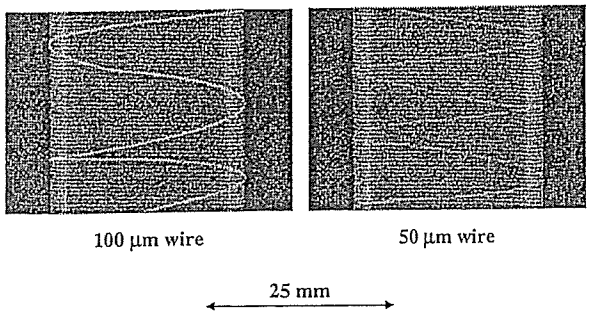

Fig. 7. Radiograms of tungsten wires coiled around PMMA pipes.

exposure time. Fig. 6 shows measured spectra from the copper target with a charging voltage of 50 kV. In fact, we observed clean K lines such as lasers, and Kα lines were left by absorbing Kβ lines using a 15-μm-thick cobalt filter. The characteristic X-ray intensity substantially increased with corresponding increases in the charging voltage, and higher harmonic hard X-rays were observed.

4. Radiography

The plasma radiography was performed by the CR system without using the filter. The charging voltage and the distance between the X-ray source and imaging plate were 50 kV and 1.2 m, respectively.

Firstly, rough measurements of spatial resolution were made using wires. Fig. 7 shows radiograms of tungsten wires coiled around pipes made of polymethyl methacrylate (PMMA). Although the image contrast decreased somewhat with decreases in the wire diameter, due to blurring of the image caused by the sampling pitch of 87.5 μm, a 50-μm-diameter wire could be observed.

Fig. 8 shows a radiogram of a vertebra, and fine structures in the vertebra were observed. Next, an image of plastic bullets falling into a polypropylene beaker from a plastic test tube is shown in Fig. 9. Because the X-ray duration was about 500 ns, the stop-motion image of bullets could be obtained.

5. Conclusions and outlook

Concerning the spectrum measurement, we obtained fairly intense and clean K lines from a weakly ionized linear plasma X-ray source, and Kα lines were left by absorbing Kβ lines using the cobalt filter. In particular, the higher harmonic X-rays were produced from the plasma. Because the X-ray intensities of the harmonics increased with increases in the charging voltage, the

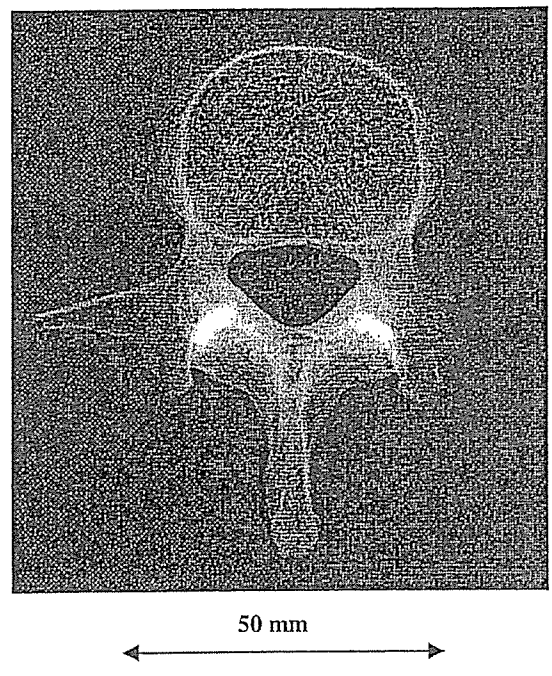

Fig. 8. Radiogram of a vertebra.

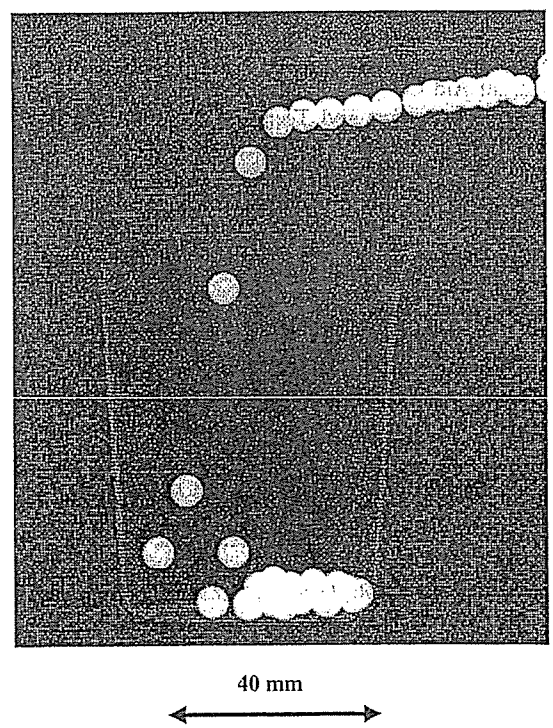

Fig. 9. Radiogram of plastic bullets falling into polypropylene beaker from a plastic test tube.

harmonic bremsstrahlung rays survived due to the X-ray resonation.

To perform monochromatic radiography, the higher harmonics are not necessary. Therefore, the condenser charging voltage should be minimized in order to decrease the intensities of higher harmonics, and the condenser capacity should be maximized to increase the characteristic X-ray intensity. On the other hand, because the intensities of harmonics increase with increases in the charging voltage, high-photon-energy monochromatic radiography may be realized.

In this research, we obtained sufficient characteristic X-ray intensity per pulse for CR radiography, and the generator produced number of characteristic K photons was approximately 1×10^8 photons/cm^2 at 1.0 m per pulse. In addition, since the photon energy of characteristic X-rays can be controlled by changing the target elements, various quasi-monochromatic high-speed radiographies, such as high-contrast angiography and mammography, will be possible.

Acknowledgments

This work was supported by Grants-in-Aid for Scientific Research (13470154, 13877114, 16591181, and 16591222) and Advanced Medical Scientific Research from MECSST, Health and Labor Sciences Research Grants (RAMT-nano-001, RHGTEFB-genome-005 and RHGTEFB-saisei-003), Grants from the Keiryo Research Foundation, the Promotion and Mutual Aid Corporation for Private Schools of Japan, the Japan Science and Technology Agency (JST), and the New Energy and Industrial Technology Development Organization (NEDO, Industrial Technology Research Grant Program in '03).

References

Ando, M., Maksimenko, M., Sugiyama, H., Pattanasiriwisawa, W., Hyodo, K., Uyama, C., 2002. A simple X-ray dark- and bright- field imaging using achromatic Laue optics. Jpn J. Appl. Phys. 41, L1016–L1018.

Davis, T.J., Gao, D., Gureyev, T.E., Stevenson, A.W., Wilkins, S.W., 1995. Phase-contrast imaging of weakly absorbing materials using hard X-rays. Nature 373, 595–597.

Germer, R., 1979. X-ray flash techniques. J. Phys. E: Sci. Instrum. 12, 336–350.

Hyodo, K., Ando, M., Oku, Y., Yamamoto, S., Takeda, T., Itai, Y., Ohtsuka, S., Sugishita, Y., Tada, J., 1998. Development of a two-dimensional imaging system for clinical applications of intravenous coronary angiography using intense synchrotron radiation produced by a multipole wiggler. J. Synchrotron. Rad. 5, 1123–1126.

Macchietto, C.D., Benware, B.R., Rocca, J.J., 1999. Generation of millijoule-level soft-X-ray laser pulses at a 4-Hz repetition rate in a highly saturated tabletop capillary discharge amplifier. Opt. Lett. 24, 1115–1117.

Momose, A., Takeda, T., Itai, Y., Hirano, K., 1996. Phase-contrast X-ray computed tomography for observing biological soft tissues. Nat. Med. 2, 473–475.

Mori, H., Hyodo, K., Tanaka, E., Mohammed, M.U., Yamakawa, A., Shinozaki, Y., Nakazawa, H., Tanaka, Y., Sekka, T., Iwata, Y., Honda, S., Umetani, K., Ueki, H., Yokoyama, T., Tanioka, K., Kubota, M., Hosaka, H., Ishizawa, N., Ando, M., 1996. Small-vessel radiography in situ with monochromatic synchrotoron radiation. Radiology 201, 173–177.

Rocca, J.J., Shlyaptsev, V., Tomasel, F.G., Cortazar, O.D., Hartshorn, D., Chilla, J.L.A., 1994. Demonstration of a discharge pumped table-top soft X-ray laser. Phys. Lev. Lett. 73, 2192–2195.

Rocca, J.J., Clark, D.P., Chilla, J.L.A., Shlyaptsev, V.N., 1996. Energy extraction and achievement of the saturation linit in a discharge-pumped table-top soft X-ray amplifier. Phys. Lev. Lett. 77, 1476–1479.

Sato, E., Kimura, S., Kawasaki, S., Isobe, H., Takahashi, K., Tamakawa, Y., Yanagisawa, T., 1990. Repetitive flash X-ray generator utilizing a simple diode with a new type of energy-selective function. Rev. Sci. Instrum. 61, 2343–2348.

Sato, E., Takahashi, K., Sagae, M., Kimura, S., Oizumi, T., Hayasi, Y., Tamakawa, Y., Yanagisawa, T., 1994a. Sub-kilohertz flash X-ray generator utilizing a glass-enclosed cold-cathode triode. Med. Biol. Eng. Comput. 32, 289–294.

Sato, E., Sagae, M., Takahashi, K., Shikoda, A., Oizumi, T., Hayasi, Y., Tamakawa, Y., Yanagisawa, T., 1994b. 10 kHz microsecond pulsed X-ray generator utilizing a hot-cathode triode with variable durations for biomedical radiography. Med. Biol. Eng. Comput. 32, 295–301.

Sato, E., Sato, K., Tamakawa, Y., 2000. Film-less computed radiography system for high-speed imaging. Ann. Rep. Iwate Med. Univ. Sch. Lib. Arts Sci. 35, 13–23.

Sato, E., Hayasi, Y., Germer, R., Tanaka, E., Mori, H., Kawai, T., Obara, H., Ichimaru, T., Takayama, K., Ido, H., 2003a. Irradiation of intense characteristic X-rays from weakly ionized linear molybdenum plasma. Jpn J. Med. Phys. 23, 123–131.

Sato, E., Hayasi, Y., Germer, R., Tanaka, E., Mori, H., Kawai, T., Ichimaru, T., Takayama, K., Ido, H., 2003b. Quasi-monochromatic flash X-ray generator utilizing weakly ionized linear copper plasma. Rev. Sci. Instrum. 74, 5236–5240.

Sato, E., Sagae, M., Tanaka, E., Hayasi, Y., Germer, R., Mori, H., Kawai, T., Ichimaru, T., Sato, S., Takayama, Y., Ido, H., 2004a. Quasi-monochromatic flash X-ray generator utilizing a disk-cathode molybdenum tube. Jpn J. Appl. Phys. 43, 7324–7328.

Sato, E., Hayasi, Y., Germer, R., Tanaka, E., Mori, H., Kawai, T., Ichimaru, T., Sato, S., Takayama, K., Ido, H., 2004b. Sharp characteristic X-ray irradiation from weakly ionized linear plasma. J. Electron. Spectrosc. Related Phenom. 137–140, 713–720.

Sato, E., Tanaka, E., Mori, H., Kawai, T., Ichimaru, T., Sato, S., Takayama, K., Ido, H., 2004c. Demonstration of